# CHARACTERIZATION OF LACTATE SENSORS BASED ON LACTATE OXIDASE AND PALLADIUM BENZOPORPHYRIN IMMOBILIZED IN HYDROGELS

A Thesis

by

LIAM P. ANDRUS

Submitted to the Office of Graduate and Professional Studies of
Texas A&M University
in partial fulfillment of the requirements for the degree of

MASTER OF SCIENCE

| | |
|---|---|
| Chair of Committee, | Michael J. McShane |
| Committee Members, | Michael V. Pishko |
| | Satish Bukkapatnam |
| Head of Department, | Gerard L. Coté |

August 2015

Major Subject: Biomedical Engineering

# ABSTRACT

An optical biosensor for lactate detection is described. By encapsulating enzymes and phosphorescent oxygen sensing molecules within permeable hydrogel materials, a lactate-sensitive change in emission lifetimes was achieved. The relative amount of monomer was varied to compare the response of the enzyme-phosphor system in three homo- and co-polymer materials: poly(2-hydroxyethyl methacrylate) (pHEMA) and two copolymers of pHEMA and poly(acrylamide) (pAam). Diffusion analysis demonstrated the ability to control lactate transport by varying the hydrogel composition, while having a minimal effect on oxygen diffusion. Sensors displayed the desired dose-variable response to lactate challenges, highlighting the tunable, diffusion-controlled nature of the sensing platform. Short-term repeated exposure tests revealed enhanced stability for sensors comprising hydrogels with acrylamide additives; after an initial "break-in" period, signal retention was 100% for 15 repeated cycles. Evaluation of long-term sensor performance revealed significant reduction in lactate sensitivity for all materials investigated. Sensor response was quickly saturated in a low oxygen testing environment, indicating further work is needed to enhance viability of platform for implantation. Finally, because this study describes the modification of a previously developed glucose sensor for lactate analysis, it demonstrates the potential for mix-and-match enzyme-phosphor-hydrogel sensing for use in future multi-analyte sensors.

ACKNOWLEDGEMENTS

I would like to thank my committee chair, Dr. McShane, and my committee members, Dr. Pishko, and Dr. Bukkapatnam for their guidance and support throughout the course of this research. Thanks also go to my friends and colleagues and the department faculty and staff for making my time at Texas A&M University a great educational experience. Finally, thanks to my family for their encouragement.

TABLE OF CONTENTS

Page

LIST OF FIGURES

Page

LIST OF TABLES

Page

LIST OF EQUATIONS

Page

# CHAPTER I

# INTRODUCTION

## 1.1 Overview

Sensors capable of rapid analyte detection are essential for improving personalized healthcare[1]. Further, the ability to accurately detect and track substrate concentrations *in vivo* allows for precise diagnosis and better management of many chronic diseases[2]. Diabetes, one such disease, affects nearly 21 million people in the U.S. and 300 million people worldwide[3]. Diabetic patients suffer from abnormally high blood glucose levels, a consequence of the bodies' inability to produce or respond appropriately to physiological levels of insulin. Therefore, patients must take daily injections in order to maintain normo-glycemia and encourage the cellular uptake of glucose, which otherwise would be toxic. Chronic hyperglycemia (high blood glucose) increases a patient's risk to various pathologies including nephropathy, retinopathy, and neuropathy[2]. Additionally, hypertension is almost twice as common in diabetics when compared to healthy patients[4].

Complications of hyperglycemia notwithstanding, acute-hypoglycemia can be problematic in its own right. Severe hypoglycemia can no doubt be fatal[5], and has been linked to both cognitive impairment and nerve cell death[6]. Three recent reports indicate that complications of hypoglycemia are responsible for 4%[7], 7%[8], and 10%[9] of deaths of patients with type 1 diabetes. Expectedly, clinical studies report significantly improved long term prognoses for patients who maintain proper control of blood glucose levels

when compared to those who do not[10]. Thus, tight control of blood glucose is essential for proper diabetes management.

Similarly, studies have shown L-lactate to be an important biomarker in many critical care[11] and clinical[12] applications. While lactate is a normal byproduct of cellular metabolism, intracellular concentrations of lactate increase more dramatically during anaerobic respiration. Interstitial lactate levels rise with anaerobia, leading to accumulation in muscles and other tissues. High concentrations of lactate are associated with muscle soreness, pain, and impaired function[13]. Therefore, lactate is useful in assessing a variety of acute deoxygenation events including hypovolemia (shock)[14], heart disease[15], and renal failure[16]. High lactate concentrations are also commonplace in traumatic injury, where a patient has undergone significant blood loss. In fact, monitoring of blood lactate is shown to improve identification of patients requiring resuscitative care (93%) when compared to standard blood pressure monitoring (67%) [11], highlighting it's potential as an accurate metric for systemic health assessment in critical care situations. Nearly all soft tissue damage is correlated to an increase in lactate[17]. This makes continuous tracking useful for dynamic monitoring of active-duty military and other high risk personnel. Further, lactate tracking can be used to approximate tissue oxygenation in endurance athletes[18], a parameter used to estimate muscle fatigue and overall fitness. Therefore a continuous lactate monitor may be used when optimal training intensities and minimal fatigue are desired.

## 1.2 Standard analyte monitoring techniques

Typically, lactate/glucose is analyzed by placing a small blood sample on a disposable electrode coated with a substrate-sensitive enzyme. The concept, originally developed by Clark et al[19] to measure oxygen tension in cardiac surgery, is the basis for most commercially available glucometers. Glucometers rely on hydrogen peroxide ($H_2O_2$) produced from the catalysis of glucose and oxygen by glucose oxidase (GOx). If subjected to a baseline current, $H_2O_2$ will dissociate, inducing a change in charge directly proportional to glucose concentration.

It is suggested that diabetic patients check their blood glucose levels 4-5 times daily. Blood sampling requires painful fingersticks and may lead to patient noncompliance, causing many patients to check blood sugars less frequently. Lactate detection is equally painful and may lead to noncompliance. Lactate is infrequently used in critical care situations even though reports indicate it to be a highly reliable biomarker for emergency health assessment[11].

Aside from being painful and inconvenient, *ex vivo* sampling does not provide caregivers or patients the ability to track systemic fluctuations over time, giving little insight into long term trends. The aforementioned facts necessitate the development of a continuous monitor, yet there remains a lack of effective techniques.

## 1.3 Continuous analyte monitoring techniques

To date, there have been a number of attempts to develop miniaturized platforms for continuous monitoring of various biochemical metabolites, most notably glucose[20]. Contemporary continuous glucose monitoring (CGM) systems rely on GOx to produce

$H_2O_2$ at the surface of an implanted electrode and the resulting change in electric potential is then correlated to interstitial glucose concentrations[20a]. Typically, a polished needle type Au/Pt electrode is exposed to a solution of GOx, glutaraldehyde, and bovine serum albumin. Glutaraldehyde is known to crosslink enzymes at surface amine groups while maintaining an active enzyme conformation, allowing for physical adsorption of the enzyme onto the electrode without substantial loss of catalytic activity. Next, the enzyme-electrode is dip-coated in a biocompatible polymer to aide in tissue integration. Functionalized electrodes may contain thin-film coatings of various materials which function as glucose-diffusion barriers. Increasing coating thickness works to mitigate enzyme saturation and therefore extend glucose-sensitive range. The same concept has also been applied to lactate sensing using the lactate-sensitive enzyme lactate oxidase (LOx)[20b].

Currently, a number of continuous glucose monitoring systems are commercially available, including Medtronic's Guardian® Real Time System, Dexcom's G4® Platinum System, and Abbott Laboratories FreeStyle™ Navigator II system. These FDA-approved devices are a major step forward when compared to *ex vivo* blood sampling. While enzyme electrodes and their various iterations have proven useful, the immune response elicited by the implant consistently leads to sensor failure. The entry wound caused by implantation initiates a chain of immune reactions beginning with inflammation, protein adsorption, and macrophage recruitment. Fibrotic encapsulation of the implanted sensor is the final defense against the foreign body. Encapsulation of the enzyme-electrode significantly alters analyte diffusion to the sensor surface, resulting in

a reduction in sensitivity. Figure 1.1 shows an illustration of the foreign body response to an implanted sensor and its effect on glucose diffusion.

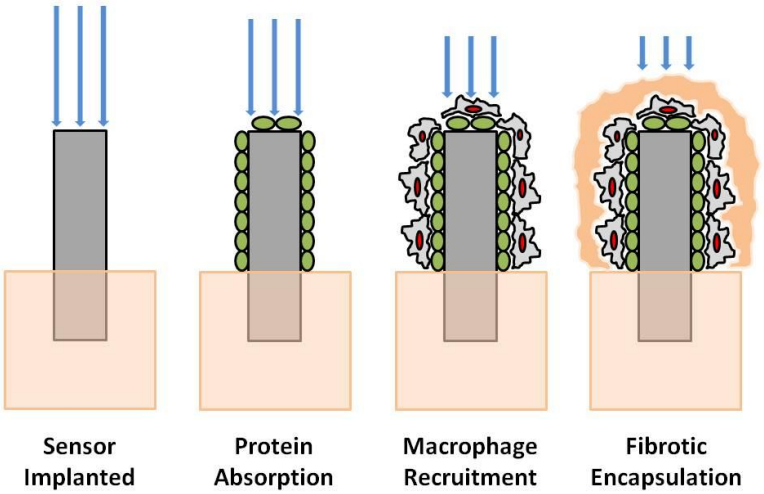


**Figure 1.1.** Illustration of foreign body response to implant

Aside from diffusion concerns, enzyme deactivation will also reduce sensitivity to glucose. $H_2O_2$ production is necessary to transmit an electrical signal across the skin. $H_2O_2$ is known to be a strong biochemical oxidizer as well as corrosive in high concentrations. $H_2O_2$ deactivates the immobilized GOx, leading to reduced production. The end result is similar to fibrotic encapsulation; a reduction in electric potential is observed at a given glucose concentration. Both of these transient effects require that CGM devices be recalibrated every few days. Current CGM devices are effective for 4-7 days before bio-fouling effects render sensors useless. Further, the implantation site provides a potential bacterial pathway, leading to an increased risk of infection.

## 1.4 Optical techniques for analyte detection

Optical techniques have been investigated for noninvasive estimation of analyte concentrations *in vivo* to avoid biocompatibility issues associated with electrochemical-based sensing modalities. Optical methods display many advantages over amperometric detection. Optical systems rely on photon transfer and detection, eliminating need of a transcutaneous connection. Previous reports have shown the feasibility of using dual-wavelength polarimetry[21], optical coherence tomography[22], and Raman spectroscopy[23] as methods to approximate various biochemistries *in vivo*. Malik et al demonstrated how rotation of plane polarized light in glucose containing solution can be used to estimate glucose levels. Vitreous humor was chosen as the testing medium, providing an easily accessible detection site. Further, utilization of dual-wavelength polarimetry reduced signal noise associated with corneal birefringence. Malik et al conducted live animal experiments, showing promise for *in vivo* glucose detection. Researchers at University of Texas Medical Branch and Texas A&M University demonstrated the use of optical coherence tomography and Raman spectroscopy as techniques for detection of either glucose or lactate. Esenaliev et al exploited glucose-dependent backscattering effects to estimate glucose concentration within tissues. Glucose is well known to reduce scattering coefficients of tissues[24]; changes in coherent backscattering were used to estimate concentrations *in vivo*, effectively creating a glucose-sensitive system. Alternatively, Caspers et al used Raman spectroscopy to provide spatially-resolved spectra of the fingertip. This study proved large variations in lactate concentration at the surface of the skin and 30 μm below. All of these systems are sensitive to lactate- or

glucose-concentration-dependent changes in emitted/scattered light. Both glucose and lactate are small, meaning biochemical signatures attributed to each can be very low depending on the technique employed. Therefore, it can be difficult to reproduce consistent results in a clinical setting due to the small intrinsic signals from target molecules. As previously noted, light is scattered by tissue, meaning localized tissue heterogeneity may lead to erroneous estimation of *in vivo* concentrations. These techniques are intensity-based, making them susceptible to differences in temperature, pH and other physiological variables which may alter flux of emitted photons.

## 1.5 Phosphorescent analyte detection

To amplify optical signals above background and interference variability in a dynamic *in vivo* environment, implantable materials are being designed as "transducers" to convert chemical concentration into a phosphorescent signal. Recently, highly sensitive phosphors have been developed and applied for biomolecular assay applications[25]. These molecules absorb and emit at wavelengths within the commonly termed "optical window" ($\lambda$=650-1350 nm), allowing for photon transmission through skin[26]. Phosphors are characterized by relatively long emission lifetimes in the µs range, compared to tissue fluorophores with nanosecond decays, meaning it is possible to discriminate these signals from background and natural fluorescence using sophisticated optical analysis techniques. As with other optical systems, strong signal-to-noise ratios are important for accurate analyte detection, making phosphors attractive for subcutaneously implanted sensors.

While there are a multitude of commercially available dyes, those displaying oxygen sensitivity are most pertinent to this work. Previous studies by McShane et al made significant contributions to the development of biosensors based on $O_2$-quenched metalloporphyrins. These reports describe glucose sensing platforms based on a number of ruthenium-and platinum-porphyrin conjugates[27]. To fabricate a glucose sensor, metalloporphyrin conjugates were co-immobilized along with GOx in various diffusion-limiting matrices. As glucose diffuses inward, oxygen is consumed by GOx. These dyes respond to $O_2$ reduction by emitting at higher phosphorescent lifetimes and intensities. Thus, by altering materials used to entrap the proposed sensing molecules, diffusion-controlled response over a wide range of glucose concentrations was realized[27a, 28]. While this platform has shown promise for glucose sensing, it's efficacy in sensing other metabolites has not been established.

## 1.6 Research objective

The goal of this thesis is to demonstrate the effectiveness of a sensing platform developed by McShane et al for alternative analyte detection, in this case *L-lactate*. Work described herein builds upon previous glucose sensing modalities[27-28]. A long emission lifetime benzoporphyrin was co-localized along with a lactate selective enzyme (LOx) within various homo- and co-polymer hydrogels to demonstrate diffusion-controlled, lactate-sensitive response over a wide range of physiologically relevant concentrations.

Freshly prepared lactate sensors were characterized by a number of commonly known sensor metrics. To investigate diffusion-controlled nature of the platform, bulk

lactate- and oxygen-transport properties were assessed. A relationship between diffusion coefficients and macro-sensor response is proposed, inferring material-dependent lactate sensitivity. Next, acute- and long-term sensor stability was evaluated in various dynamic storage conditions to assess suitability of materials for immobilization of sensing chemistry. Afterwards, sensors were evaluated in a low $O_2$ environment to better understand *in vivo* performance capabilities.

Finally, this works illustrates the general applicability of the enzyme-benzoporphyrin-hydrogel platform for alternative analyte analysis. While initially purposed for glucose detection, substitution of a discrete, lactate-specific enzyme within diffusion-tailored hydrogels shows the device's potential as a multi-analyte sensing platform.

## 1.7 Chapter organization

This thesis is organized as follows:

Background is sectioned into three parts. The first section includes theory and applications for enzymatic-based sensing modalities as well as recent advances that explore the utilization of lactate-selective enzymes for optical detection of lactate. Next, long emission lifetime metalloporphyrin complexes relevant to the given application are discussed, with attention given to the theory of phosphorescent emission lifetime and porphyrin sensitivity to oxygen quenching. Afterwards, a review of hydrogel biocompatibly is given, specifically those materials used by previous groups for enzyme immobilization. Finally, theory to quantitatively describe molecular transport through materials is presented.

Studies of previous diffusion-controlled sensing modalities developed by McShane and others are reviewed to better understand overall approach. A brief discussion will help to understand how these past studies relate to the material presented here.

Materials and Methods presents all relevant precursor materials needed to produce sensors as well as comprehensive synthesis techniques. A bench-top testing apparatus is described, with special attention given to flow cell design. Instrumentation used to interrogate sensors, relevant sampling techniques, and methods to evaluate optical response at ambient and low $O_2$ conditions are described. Sensor performance is evaluated by determining analytical range, sensitivity, total change in lifetime, and response time. Additionally, techniques to assess lactate and $O_2$ transport through each material are presented. Finally, a description is given of two experimental setups designed to test acute- and long-term sensor stability.

Results and Discussion presents studies' findings and includes discussion of possible implications. First, design of a flow cell used in sensor evaluation is presented along with a description of fabrication techniques. Next, lactate and oxygen diffusion profiles of each material are presented and discussed. Optical response to step increases in bulk lactate are presented and evaluated. Variability in homo- and co-material diffusivity is compared to optical response to highlight the tunable nature of the platform. Analysis of acute- and long-term stability is done to evaluate suitability of materials for immobilization of proposed sensing chemistry.

Conclusions and Future Work details closing remarks on sensor viability and efficacy as an implantable device. Preliminary results on sensor response within a low oxygen environment evaluate possible *in vivo* capabilities. Implications of these results are discussed in relation to sensor response at ambient oxygen. Conjecture on potential methods to accurately tune sensor response at low oxygen as well as techniques to improve enzyme stability are discussed. Finally, general applicability of sensor platform for sensing of multiple substrates and future applications are presented.

References include reports by previous groups which help to understand the presented work.

# CHAPTER II

# BACKGROUND AND SIGNIFICANCE

## 2.1 Enzymatic sensing techniques

### 2.1.1 Theory

In the field of medical diagnostics, a sensing platform capable of real-time *in vivo* analyte tracking has been sought after for decades. Recently, there have been a number of attempts to develop miniaturized platforms for continuous monitoring of various biochemical metabolites[20]. Many of these devices rely on an electrochemical sensing assay for metabolite detection. Typically, an oxidoreductase enzyme catalyzes oxygen along with another substrate. Equation 2.1 describes kinetics of an oxidoreductase enzyme in the presence of substrate and $O_2$.

$$E_{ox} + S \overset{k_1}{\Rightarrow} E_{red}X_1 \overset{k_2}{\Rightarrow} E_{red} + P$$

$$E_{red} + O_2 \overset{k_3}{\Rightarrow} E^*_{ox}X_2 \overset{k_4}{\Rightarrow} E_{ox} + H_2O_2$$

**Equation 2.1.** Kinetics of generic oxidoreductase

where $E_{ox}$ and $E_{red}$ are the oxidized and reduced form of enzyme $E$, $S$ is the substrate, $P$ is a byproduct, $E_{red}X_1$ is the reduced enzyme-substrate complex, $E^*_{ox}X_2$ is the oxidized enzyme-substrate complex, and $k_1$, $k_2$, $k_3$, $k_4$ are the reaction rate constants. For electrochemical-based methods (e.g. contemporary continuous glucose monitors), $H_2O_2$ production is assumed to be the direct result of the electro-reduction/oxidation of the substrate $S$. $H_2O_2$ readily oxidizes metal, making it possible to measure electric potential

across a subcutaneously implanted electrode. Similar approaches have been investigated for lactate sensing[29]. As is the case with GOx and glucose, lactate/$O_2$ catalysis is possible with the oxidoreductase enzyme lactate oxidase (LOx). LOx catalyzes the reduction of molecular $O_2$ by lactate. Kinetics of LOx are described by equation 2.2.

$$E_{ox} + lactate \overset{k_1}{\Rightarrow} E_{red}X_1 \overset{k_2}{\Rightarrow} E_{red} + pyruvate$$

$$E_{red} + O_2 \overset{k_3}{\Rightarrow} E^*_{ox}X_2 \overset{k_4}{\Rightarrow} E_{ox} + H_2O_2$$

**Equation 2.2.** Kinetics of lactate oxidase

where $E_{ox}$ and $E_{red}$ are the oxidized and reduced form of LOx, $E_{red}X_1$ is the LOx-lactate complex, $E^*_{ox}X_2$ is the LOx-$O_2$ complex, and $k_1$, $k_2$, $k_3$, $k_4$ are the reaction rate constants. While electrochemical lactate sensors rely solely on $H_2O_2$ production, optical devices can detect either $H_2O_2$ production or $O_2$ consumption. Thus, production or consumption of either chemical can be used to transmit an optical signal.

2.1.2 Recent advances

A number of enzyme-based sensing modalities for amperometric detection of lactate have been reported[20b, 29b]. Thomas developed a contact lens functionalized to detect lactate in vitreous humor. Poly(ethylene terepthalate) wafers were cut to size and thoroughly cleaned. Next, a Clark-type Pt electrode was lithographically patterned onto the wafer surface. A solution containing LOx, glutaraldehyde, and bovine serum albumin was mixed and deposited onto the surface of the electrode-wafer. Finally, functionalized wafers were dip-coated in polyurethane (PU) and dried overnight.

Exposure to lactate produced a measureable current, thus displaying sensitivity. Although the device required a physical connection to a receiver, the authors promised the integration of wireless transmission to be described in future studies. Only then would it be effective for everyday use.

Other groups have successfully used optical techniques to detect lactate[20b, 30]. Marquette et al were able to couple LOx and a peroxide sensitive fluorophore, luminol, to the end of an optical fiber bundle[31]. Upon exposure to lactate, sensors demonstrated an increase in fluorescent intensity due to $H_2O_2$ oxidation of the co-localized luminol. This technique provided high sensitivity, although a narrow analytical range (30 pmol). In other studies, Hu et al developed highly fluorescent cupric oxide nano-particles functionalized with terephthalic acid, a substrate in peroxidase catalysis. Nano-particles displayed enzyme mimetic characteristics, albeit with more stable activity than seen in natural peroxidase[29c]. By coupling this $H_2O_2$-sensitive system with LOx, a lactate specific fluorescent nano-sensor was developed. Both of these methods displayed narrow lactate detection ranges, much lower than the typical 0-2 mMol lactate of healthy human serum.

Alternatively, Trettnak et al developed a lactate sensor by monitoring oxygen consumption as a function of lactate concentration. This was accomplished by co-localizing LOx and an $O_2$-sensitive fluorophore, decacyclene [32]. LOx and solubilized decacyclene were covalently bound to nylon 6-6 membranes which were then attached to a fiber optic bundle. Upon lactate exposure, sensors emitted high fluorescent intensities due to the decrease in available oxygen and subsequent decrease in

fluorescent quenching. Dremel et al described a similar $O_2$-sensitive modality for detection of L-lactic acid in food products[33]. With proper preconditioning of fluorescent sensing chemistry, continuous lactate analysis was possible for ≥2 days.

These reports show the possibility of optical lactate detection, yet *in vivo* capabilities were hardly considered. Again, intensity-based measurements are susceptible to physiological changes in pH, temperature, and subcutaneous environment, making sensors unreliable if tissue heterogeneity exists near the implantation site. Therefore, alternative techniques should be explored in order to develop a more robust sensing mechanism.

## 2.2 Long lifetime metalloporphyrins

### 2.2.1 Theory

To reduce signal variability seen in intensity-based measurements, emission lifetime can be used as a means to sensitively interrogate implants. Emission lifetime is defined as the average time a molecule will stay in its excited state after photon absorption. Upon excitation, electrons in the highest occupied orbital are excited to the lowest unoccupied orbital and beyond. After some time, electrons "relax" to a ground state, in the process emitting photons of different wavelengths. Re-emission is not instantaneous due to various radiative and non-radiative transitions. Fluorescent lifetime is defined as the average time a molecule takes to return to ground after excitation to a singlet energy state. This transient reduction in intensity can be measured as voltage decay across a detector. Using equation 2.3, a decay curve can be approximated.

$$[X]_t = [X_0]e^{-\Gamma t}$$

**Equation 2.3.** 1st order decay

where $[X]_0$ and $[X]_t$ are the concentrations of excited molecules initially and at time *t*, respectively, and $\Gamma$ is the decay rate. Emission lifetime, $\tau$, is defined as the inverse of $\Gamma$. Lifetime is an intrinsic property and thus does not depend on the method of measurement. It is also a state function, independent of excitation wavelength and duration of light exposure. Additionally, lifetime measurements are mostly independent of intensity measurements[34] within a range of fluorophore concentrations.

As mentioned previously, there are number of internal non-radiative processes which can cause a delay in photon emission. Vibrational relaxation is the simplest of these transitions. After photon absorption, a molecule rapidly relaxes to the lowest vibrational state within its current excited energy level; this is observed as a change in intra- or inter-molecular kinetic energy. It is also possible for an excited electron to transition from a vibrational energy level in one energy state to another vibrational level in a lower energy state. Unlike vibrational relaxation, internal conversion involves a change in electronic state and is more likely to occur if there is significant overlap between vibrational and electronic energy levels. An additional non-radiative transition (and perhaps most important to this work) is intersystem crossing. This is the slowest of the transitions shown in the Jablonski diagram in figure 2.1. Intersystem crossing is a transition from one electronic state to another with a different spin multiplicity. In a singlet state, an excited electron is paired with a ground state electron of opposite spin. Intersystem crossing occurs when an excited electron undergoes spin reversal. This

triplet state is considered a "forbidden transition" and typically occurs less frequently. The radiative emission between an excited triplet state and ground state is commonly referred to as phosphorescence. The timescale of phosphorescent decay is typically much longer than fluorescent decay. Certain phosphors are characterized by exceptionally long lifetime decays in the μs-ms range[35].

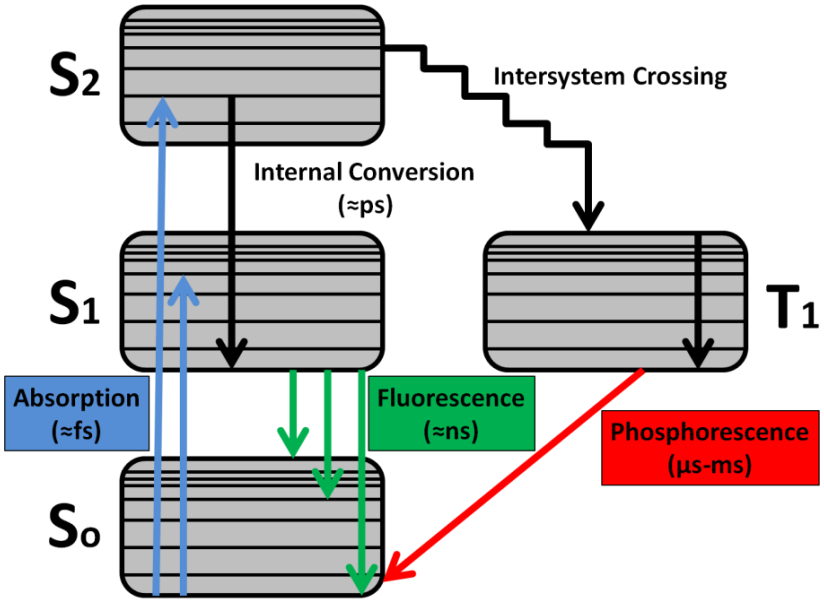


**Figure 2.1.** Jablonski diagram

Some phosphors are sensitive to quenching by molecular $O_2$. If $O_2$ concentrations are high, energy absorbed from a photon is transferred through $O_2$ molecules to an electronic ground state rather than being re-emitted as another photon. Thus, phosphorescent intensity and emission lifetime profiles can be related to oxygen concentration. This is described by the Stern-Volmer relationship.

$$\frac{\tau_0}{\tau} = \frac{I_0}{I} = 1 + K_{sv}[O_2]$$

**Equation 2.4.** Stern-Volmer relationship of fluorescence/phosphorescence

where $\tau_0$ and $I_0$ are phosphorescent lifetime and intensity in absence of $O_2$, $\tau$ and $I$ are lifetime and intensity, $K_{sv}$ is the phosphor specific Stern-Volmer constant, and $[O_2]$ is oxygen concentration.

2.2.2 Recent advances

A number of groups have conjugated porphyrin compounds with various metal atoms to produce dyes with exceptionally long phosphorescent lifetimes[25a, 25c, 35-36]. O'Riordan et al developed a series of Pd(II)- Pt(II)-co-proporphyrin I derivatives for *in vitro* labeling of various antibodies[25a]. Activity and stability analyses were performed on antibody-dye conjugates as well as on unlabeled antibodies. Similarly, O'Sullivan et al described a method of tagging oligonucleotides with Pt(II) co-proporpyhrins[25c]. Purification via HPLC and absorption spectra of compounds were done to characterize the developed probes. As is the case with most fluorescent imaging probes, high emissions must be maintained to ensure accurate time-resolved measurements. Therefore, $Na_2SO_3$ was added as a deoxygenator to reduce molecular $O_2$ quenching effects.

While sensitivity to oxygen may be problematic for protein binding applications, it is useful in sensor development. Niedermair et al developed a number of $O_2$-sensitive near infrared Pt(II)- Pd(II)-benzoporphyrins[35a] which displayed peak excitations within the commonly termed "optical window" (λ=650-1350 nm); wavelengths with low absorption in hemoglobin (UV) and water (IR). Auto-fluorescence of tissue is relatively low and scattering effects are deemed the most important light-tissue interaction, allowing for rapid penetration through the skin. This makes the developed dyes attractive for subcutaneously implanted sensors. The benzoporphyrin used in this study is a derivative of a phosphor developed by Niedermair et al. Palladium (II)-tetramethacrylate-benzoporphyrin (BMAP) was donated by Soya Gamsey of PROFUSA (PROFUSA, San Francisco, CA, Patent WO 1998003512 A1). BMAP structure and emission spectra are shown in figure 2.2.

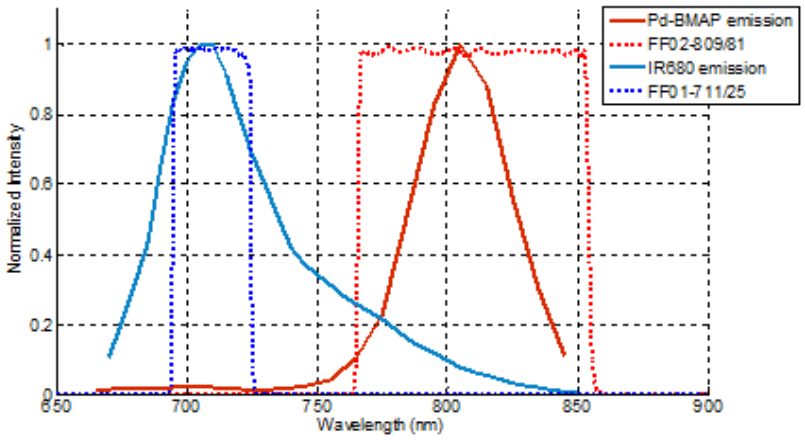


**(a)**

**Figure 2.2.** (**a**) Structure of BMAP (**b**) emission spectra of BMAP at 633 nm excitation

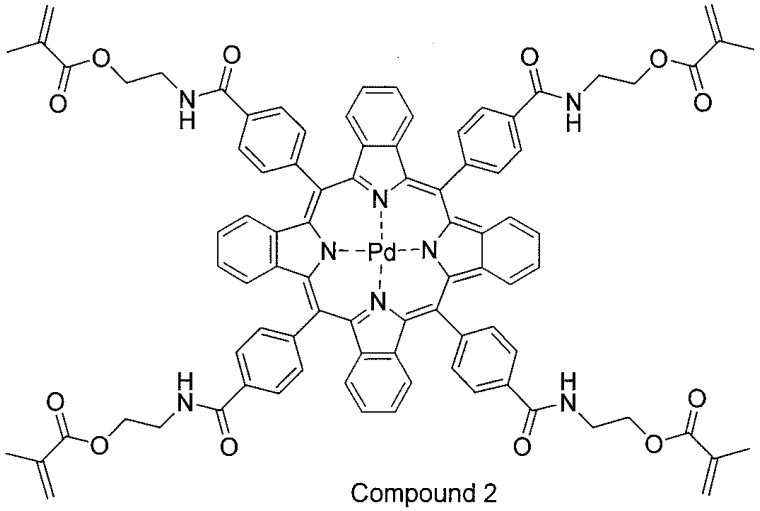


**(b)**

**Figure 2.2., Continued** (**a**) Structure of BMAP (**b**) emission spectra of BMAP at 633 nm excitation

A covalently bound central Pd atom acts as an oxygen binding center, similar to the Fe atom found in hemoglobin. In ambient conditions, emission intensities remain low due to de-excitation via energy transfer to $O_2$ by collisional quenching; this means that incident photon energies are non-radiatively transferred through $O_2$ to ground state rather than being emitted as phosphorescence. BMAP displays excellent storage stability in powder or solution form. Absorption spectrum was determined using 1 H NMR (300 Mhz, $CDCl_3$). Spectral analysis was done at room temperature and ambient $O_2$. Excitation at $\lambda = 633$ nm gave $\lambda_{peak} = 805$ nm emission, indicating a large Stokes shift and the possibility of deep tissue penetration for *in vivo* analyte analysis.

In this work, BMAP and LOx were co-localized to create a lactate-selective sensor. As previously noted, LOx activity is a function of lactate and oxygen

concentration. As lactate levels are increased, more oxygen is consumed. BMAP is highly sensitive to oxygen quenching, meaning localized oxygen concentrations can be estimated by phosphorescent intensity and emission lifetime profiles. Therefore, estimation of lactate concentration is possible by monitoring the $O_2$ quenching kinetics of BMAP in an enzyme-controlled $O_2$ micro-environment.

LOx and BMAP comprise the proposed sensing chemistry, yet alone they do little to account for the development of a functional sensor. LOx is quickly saturated at lactate concentrations found *in vivo*. Likewise, the effective optical signal is also saturated at low lactate levels. Further, co-localization of sensing chemistry is needed in order to prevent leaching. These facts highlight the need for a suitable immobilization matrix to limit diffusion and realize a functional sensor.

## 2.3 Hydrogel materials

### 2.3.1 Theory

Hydrogels may be used to entrap and control substrate diffusion to the aforementioned sensing molecules. Small molecule transport depends on a material's molecular weight, cross-link density, swelling profile in water, and polymer-molecule interaction[37]. To evaluate a diffusion coefficient, $D_L$, Fick's 2nd law of diffusion is used.

$$\frac{\delta c}{\delta t} = D_L \frac{\delta^2 c}{\delta x^2}$$

**Equation 2.5.** Fick's 2nd law of diffusion

where $c$ is concentration of substrate in the hydrogel, $D_L$ is the diffusion coefficient, and $x$ is distance. This partial differential equation models diffusion as a function of substrate concentration in bulk solution.

$O_2$ transport can be assessed indirectly via evaluation of Stern-Volmer quenching kinetics of an $O_2$-sensitive phosphor immobilized within the hydrogel. It is assumed that phosphor entrapped within a hydrogel will display different quenching properties than free phosphor, thus indicating a change in oxygen availability. If $K_{sv}$ values determined for immobilized phosphors differ from those found in free solution, material-dependent profiles can be determined. Comparison of $K_{sv}$ values may be used to assess relative oxygen permeability of selected materials.

### 2.3.2 Recent advances

To functionalize sensing chemistry into a useful biosensor, immobilization within a bioinert matrix is necessary. Hydrogels have been used extensively for *in vivo* applications due to their low toxicity and bio-fouling properties[37]. Hydrogels typically display high swelling ratios, with some able to take on 99% of their weight in water. Degradation of polymer matrix is highly dependent on repeat unit linkage. Some ester-linked polymers (such as poly(lactic-co-glycolic acid)) degrade rapidly while others display resistance to linkage-hydrolysis[38]. Degradable materials are attractive for controlled-drug release applications[39], however can be difficult for enzyme-based biosensors. If materials degrade quickly, frequent recalibrations are required to account for changes in small molecule transport, limiting their long term functionality. Therefore

it is necessary to employ mechanically robust and biointert polymers for enzyme-based applications.

Two materials, poly(2-hydroxyethyl methacrylate) (pHEMA) and poly(acrylamide) (pAam) are synthetic polymers used in numerous biomedical devices. pHEMA has been widely used in soft contact lenses[40], drug delivery systems[41], and tissue engineering constructs[42]. pHEMA is attractive due to its low cytotoxicity and biofouling properties[43]. pHEMA's ability to swell in water without losing mechanical integrity makes it an ideal material for *in vivo* applications[44].

Similarly, poly(acrylamide) (pAam) has many uses, initially purposed as a separation medium in gel electrophoresis[45]. Like pHEMA, pAam's hydrophilic nature and low biofouling properties make it suitable for *in vivo* applications[46]. Further, both pHEMA and pAam have been investigated for immobilization of enzymes and other indicator molecules in a number of biosensors[27a, 28]. Previous work has reported that crosslinking enzymes within these hydrogels can enhance catalytic stability[47]. Thus, homogenous distribution of sensing chemistry within a biocompatible gel is attractive for enzyme based sensing applications.

## 2.4 Current trends in optically active, enzyme-based hydrogel materials for analyte detection

Recently, a number of groups have reported on the development of hydrogel-based enzymatic phosphorescent biosensors[27-28, 48]. One approach developed by McShane and Brown et al used calcium alginate gel microspheres as a medium for a phosphorescent glucose sensing chemistry[48b]. Microspheres were prepared following a

procedure modified from Wan et al[49]. Briefly, a solution of 3 wt. % sodium alginate and 50 mg GOx was added to iso-octane to create water-in-oil emulsion droplets. After mixing at 5000 rpm for 10 minutes in an overhead stirrer, 10 wt. % calcium chloride solution was pipetted into the emulsion to slowly crosslink alginate. Afterwards, microspheres were rinsed and suspended in distilled water. Microsphere-enzyme conjugates were then exposed to a buffer solution (pH=12) containing an $O_2$-sensitive phosphor, ruthenium (II) tris(4,7- diphenyl-1,10-phenanthroline). Electrostatic coupling of the cationic phosphor and the anionic microspheres allowed for precipitation of dye into the alginate matrix. Afterwards, alternately charged polyelectrolyte nano-films were assembled onto microspheres. Previous studies report on highly accurate nano-film deposition onto colloidal surfaces[50]. This deposition technique allows for precise control over sensor diffusion properties, thereby allowing for control over sensor response to bulk glucose.

Microspheres were interrogated by glucose challenges using a bench-top flow through system. Incoming glucose and oxygen was consumed by GOx, and optical response was transmitted as a change in phosphorescent intensity of the immobilized phosphor. Sensors responded linearly up to 140 mg/dL glucose, yet coverage of the entire physiological range was not achieved due to high glucose diffusion. Enzymatic production of $H_2O_2$ led to GOx deactivation. Additionally, photobleaching was a major concern, and required extensive correction when processing data.

Another approach developed by McShane and Stein et al incorporated a similar sensing chemistry into functionalized microcapsules[48a]. This approach used calcium

carbonate microparticles as sacrificial templates for the fabrication of hollow polyelectrolyte microcapsules. Initially, GOx and horseradish peroxidase (HRP) were added to a $CaCl_2$ concentrated aqueous solution. HRP is a peroxidase which catalyzes $H_2O_2$ into water and $O_2$. By co-immobilizing HRP alongside GOx, it was possible to eliminate $H_2O_2$ from the system, thereby enhancing GOx stability. Next, $Na_2CO_3$ was rapidly added to the mixture to induce crystallization of $CaCO_3$ microparticles. Bi-enzyme loaded particles were rinsed and re-suspended in buffer solution. Afterwards, microparticles were subjected to polyelectrolyte nano-film deposition as described previously. Following adsorption of polyelectrolyte films onto the surface of particles, ethylenediaminetetraacetic acid (EDTA) was added to dissolve calcium core, thereby creating a hollow capsule containing both GOx and HRP.

SEM images were taken of particles in the absence of enzymes, co-precipitated particles, and the resulting microcapsules. Intra-capsule enzyme concentration was determined using both fluorescence analysis and a Bradford protein assay. Additionally, enzyme release profiles were investigated to determine stability of sensing modality.

Recently, McShane's group has immobilized a phosphorescent glucose sensing chemistry within various bioinert hydrogel matrices[27a, 28]. Generally, 2-hydroxyethyl methacrylate (HEMA) has been used as the primary monomer for enzyme-dye immobilization. Roberts et al polymerized GOx and catalase alongside Palladium (II) meso-tetra(4-carboxyphenyl) porphine (PdP) in a pHEMA matrix. Similar to HRP, catalase catalyzes $H_2O_2$ into water and $O_2$, effectively enhancing sensor stability. Initially, an aqueous solution containing GOx or GOx/catalase and a dimethyl sulfoxide

(DMSO) solution containing PdP are made and set aside. Separately, a polymer precursor solution containing HEMA, ethylene glycol, and tetraethylene glycol dimethacrylate (TEGDA) was made and vortexed. Ethylene glycol acts as a co-solvent, while TEGDA was used to crosslink the monomer. Immediately prior to photopolymerization, 2,2-dimethoxy-2- phenyl-acetophenone (photoinitiator) was added to precursor solution. Finally, GOx/catalase and PdP solutions were combined and gently mixed. Precursor solution was pipetted into a premade mold and polymerized under UV light. Afterwards, GOx was crosslinked using 1- ethyl-3-(3-dimethylaminopropyl)carbodiimide hydrochloride and N-hydroxysuccinimide.

Sensors were tested for glucose sensitivity using the bench-top testing system mentioned previously. Results indicated a largely linear response up to 225 mg/dL glucose for GOx-only sensors. Addition of catalase resulted in decreased sensitivity and a corresponding increase in analytical range (0-311 mg/dL glucose), thus enhancing sensor stability while maintaining adequate sensitivity in the physiological relevant glucose range. This work is promising, however long term stability and repeatability were not discussed.

# CHAPTER III

# MATERIALS AND METHODS

## 3.1 Materials

Catalase, ethylene glycol, 2,2-dimethoxy-2-phenyl-acetophenone (DMAP),1-Ethyl-3-[3-dimethylaminopropyl] carbodiimide hydrochloride (EDC), and sodium lactate were purchased from Sigma-Aldrich® (St. Louis, MO). Dimethyl sulfoxide (DMSO) was purchased from VWR® (Radnor, PA). Sodium chloride, potassium phosphate (dibasic), and potassium chloride were purchased from VWR® (Radnor, PA). Sodium phosphate (monobasic) was purchased from ACROS Organics™ (ThermoFisher Scientific Inc®, Waltham, MA). 2-hydroxyethyl methacrylate (HEMA) and tetra(ethylene glycol) methacrylate (TEGDMA) were purchased from Polysciences Inc™ (Warrington, PA). Lactate oxidase from *Aerococcus viridians* (LOx), acrylamide (Aam), and sulfo-N-hydroxysuccinimide (sulfo-NHS) were purchased from A.G. Scientific™ (San Diego, CA), AMRESCO® (Solon, OH), and G Biosciences™ (St. Louis, MO) respectively. Palladium (II) tetramethacrylated benzoporphyrin (BMAP) was donated by PROFUSA Inc., (San Francisco, CA). All chemicals were reagent grade and used without further purification.

## 3.2 Sensor preparation

To synthesize gels, 2.5 mg DMAP was weighed into a micro-centrifuge tube. 67.2 v/v% concentration of Aam was dissolved in DMSO separately. 250 µL monomer precursor (containing the proper v/v% ratio of HEMA to Aam solution plus 5 µL TEGDMA) was added to DMAP and vortexed. Next, 90 µL ethylene glycol was added

as a co-solvent and vortexed again. 50 µL of 10 mM BMAP solution in DMSO was added along with 125 µL LOx/catalase solution (pH=7.4) in a 10:1 molar ratio. Both dye and enzyme solutions underwent repeated pipetting to ensure proper mixing. Sensors were made with three different co-polymer materials: 75:25 pHEMA:pAam, 90:10 pHEMA:pAam and pure pHEMA. Resulting solutions were pipetted into a premade mold (consisting of a 0.03" spacer sandwiched between two clean microscope slides) and polymerized under UV light. Gel slabs were removed from molds and placed into a 15 mg sulfo-NHS and 6.6 mg EDC buffered solution. Enzyme cross-linking was done overnight at 4 C˚. After thorough rinsing, sensors were stored in fresh PBS at 4 °C in foil-covered centrifuge tubes to limit photobleaching of BMAP. 5 mm sensor strips were cut and rinsed prior to testing.

### 3.3 Bench-top testing system

A custom flow-through system was used to validate *in vitro* sensor response. Two positive displacement VICI® M6 liquid pumps (Valco Instruments™ Inc., Houston, TX) are connected to reservoirs containing either a highly concentrated (20 mM lactate) solution or phosphate buffered solution (PBS) (0 mM lactate). A LabVIEW™ program controls flow rates from both pumps independently. Flow from reservoirs is mixed prior to reaching a specially designed flow cell in which four sensors are immobilized. In a typical experiment, three lactate sensors and a pHEMA-BMAP oxygen sensor were placed in the flow cell for simultaneous monitoring. Lactate concentrations were increased every hour to ensure stable responses were achieved. Solution is flowed at a rate of 4 mL/min through the system. Discrete lactate challenges,

coined as “flight plans”, consist of progressively higher concentrations ran in series before a return to baseline. A schematic of the experimental setup is shown in figure 3.1. Custom flow cells were fabricated to secure sensors during experimentation; advantages and limitations of designs are discussed in section 4.1. All testing was performed at 37 C˚.

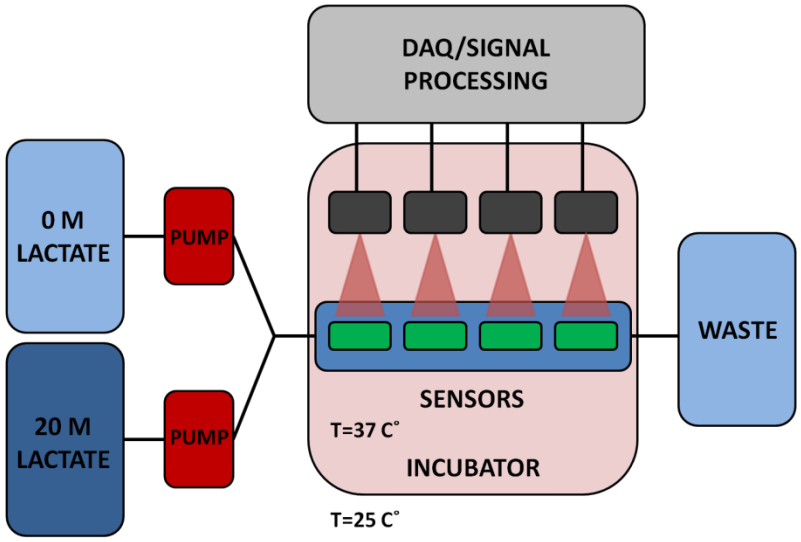


**Figure 3.1.** Illustration of flow through system (adapted from Andrus et al, 2015)[51]

Sensors were interrogated using a custom optical instrument. This instrument uses a Lumileds Luxeon Rebel red LED excitation source (Phillips®, Amsterdam, NL). The LED has peak intensity at $\lambda_{typ}$=627 nm and a bandwidth of ≈25 nm, giving it a relatively narrow emission spectra. A wide (125˚) viewing angle, as is seen here, is common among most LEDs. LED is rated to 700 mA and operated at 200 mA. Emission spectrum was confirmed spectroscopically with a peak at λ=633 nm. A FF01-631/36 excitation filter (Semrock™, Rochester, NY) is used to ensure proper emission bandwidth. Upon phosphor excitation, emitted photons are collected with a ball lens

situated at 8mm distance from the LED port; this light is collimated and passed through a FF02-809/81 emission filter (Semrock™ ) prior to detection with a Si PMT (SensL™, Cork, IR). The filter's bandwidth is nearly equal to BMAP emission spectra, ensuring likelihood of strong SNR. The entire system is contained within a miniaturized 1.5" diameter plastic casing; each such "reader head" interrogates a single sensor of interest. A LabVIEW™ program controls LED intensity, pulse on/off parameters, data acquisition, and emission lifetime calculation from the measured decays as described below.

### 3.4 Data analysis

Emission lifetimes were obtained by monitoring voltage decay across the Si PMT. Peak intensity was measured immediately following a 500 μs LED pulse. Sampling of voltage was delayed for 7 μs to reduce interference from the LED excitation pulse. Background voltage was calculated as the average intensity of the last 20% of the decay duration (2500 μs). Emission lifetime decay curves were found by averaging 128-256 acquired intensity decay profiles. Acquisitions between t = 507 μs and t = 2500 μs were repeated quickly, generally taking 1.3 seconds per cycle. Collected data were fit to the exponential in equation 2.3 using a nonlinear least squares Levenberg-Marquardt algorithm. Parameter bounds of the exponential fit limit long lifetime intensities to 0-3 V. From these averaged exponential decays lifetime, $\tau$, and long lifetime intensity are found.

A number of commonly used performance metrics were used to assess sensor response. After exposing sensors to an initial lactate challenge, adjustments were made

to modulate sensors within a more appropriate range. Specifically, adjustments to lactate concentrations were done to collect many points within the sensitive range; this allows creation of reliable calibration curves. Focus was given to four performance characteristics: sensitivity, analytical range, change in lifetime, and response time. Sensitivity is found as the linear slope of each calibration curve. Analytical range is the span over which sensitivity is maintained, defined as the interval between upper and lower limits of detection ($LOD_{high}/LOD_{low}$). Emission lifetimes at 0 mg/dL lactate plus (+) 3σ are used to calculate $LOD_{low}$. Similarly, $LOD_{high}$ is found from emission at enzyme saturation minus (-) 3σ. Change in emission lifetime is calculated as the entire range of τ between 0 mg/dL and sensor saturation. Response time refers to lag between lactate input and steady sensor response. Response time is found by averaging temporal differences between τ-3σ and τ+3σ of the previous step for the initial three steps of each flight plan. Analytical range, sensitivity, change in lifetime, and response time were calculated for n=3 sensors and metrics are reported as average ±95% CI.

### 3.5 Diffusion analysis

A horizontal diffusion cell system was used to assess lactate transport in sensor materials following procedures detailed in previous work[28]. Briefly, sensors were prepared as described in section 3.2, except that materials were polymerized in a 0.01" glass mold; the thinner samples allowed for more rapid experimentation. Sensors were preconditioned in a 60 C˚ water bath for 10 days in order to completely deactivate immobilized LOx. A lactate flight plan was monitored prior to diffusion experiments to verify enzyme deactivation. Deactivation of LOx mitigates lactate consumption concerns

and ensures reliable analysis of diffusion kinetics. A schematic of the experimental setup is shown in figure 3.2.

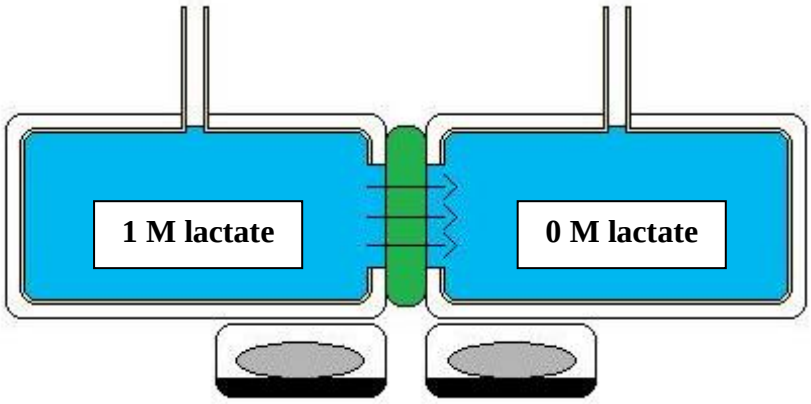


**Figure 3.2.** Illustration of diffusion cell setup

7-mm sensor punches were sandwiched between two 7 mL reservoirs. Feeder reservoirs contain 1 M lactate solution, while permeate reservoirs contain PBS solution. 100 µL samples were taken from each reservoir and replaced with fresh PBS over several hours. Samples were analyzed with a 2700 Select Biochemistry Analyzer (YSI Inc™, Yellow Springs, OH). Rates of change, *dc/dt*, were found by plotting lactate concentrations in permeate reservoirs over time; *dc/dt* was estimated as the slope of a linear fit to these data. To calculate a diffusion coefficient, $D_L$, Fick's 2nd law of diffusion was used, with the assumption that $c_{lac}(0)=$ at $t(0)$ in the permeate reservoir and homogenous mixing in each,

$$D_L = \frac{dc}{dt}\left(\frac{bV}{\emptyset}\right)$$

**Equation 3.1.** Solution of Fick's 2nd law for diffusion coefficient

where $D_L$ is the diffusion coefficient of lactate in $cm^2/s$, *dc/dt* is change in permeate reservoir concentration over time, *b* is thickness of gel, *V* is the ratio of volume of reservoir to area of gel exposed to solution, and $\phi$ is the partition coefficient. $\Phi$ is assumed to be 1 in every calculation, meaning relative $D_L$ values are reported. Although not absolute values, the calculated $D_L$ values provide insight into relative changes in diffusion; these are deemed appropriate for the purposes of this study. n=3 sensors were tested at 25 $C^{\circ}$ and $D_L$ is reported as an average.

Quenching profiles of immobilized BMAP were analyzed to assess $O_2$ transport in sensor materials. Compressed air and $N_2$ gas were bubbled into 1 L PBS to evacuate $O_2$ prior to reaching a flow cell containing n=3 sensors plus a pHEMA-BMAP oxygen reference. A 1179A mass flow controller and a pressure gauge, model PR 4000F (MKS Instruments™, Andover, MA) control $N_2$ and compressed air flow out of submerged bubbler probe and dissolved $O_2$ is externally verified with an $O_2$ microsensor (UniSense™, Aarhus, DK). Oxygen was decreased in a stepwise manner at concentrations of 210 µm, 105 µm, 52.5 µm, and 21 µm. After, flow cells were loaded with 8M glucose and 30 µM GOx solutions to consume any remaining oxygen. Flow cells were sealed and emissions were monitored overnight, allowing for detection of $\tau_0$. A value for $K_{sv}$, described by the Stern-Volmer relationship detailed in equation 2.4, is defined as the linear fit of $\tau_0/\tau$ vs. $[O_2]$. n=3 sensors were tested at 37 $C^{\circ}$ and $K_{sv}$ is reported as an average. A schematic of the experimental setup is shown in figure 3.3.

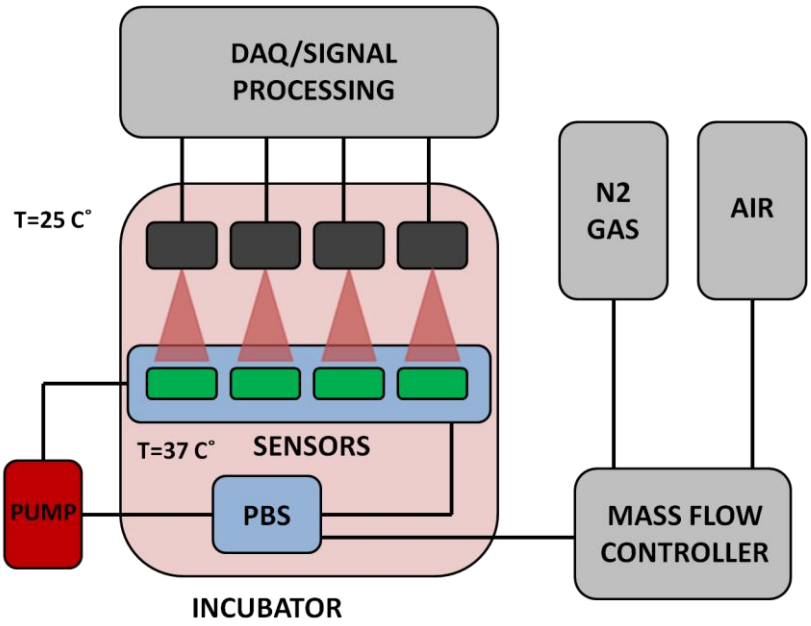


**Figure 3.3.** Illustration of oxygen testing system

## 3.6 Acute stability

Sensors were subjected to 20 consecutive lactate challenges to evaluate acute signal retention. Lactate challenges were adjusted to normalize enzymatic consumption rates within each material, meaning flight plans were determined based on the unique upper limits of detection ($LOD_{high)}$. Flight plans range between 0 mg/dL and the predetermined $LOD_{high}$ of each sensor material. "Flight plans" were run in series, with a return to baseline between each cycle. Afterwards, signal loss was calculated as percent change in emission lifetime from the initial (cycle 1) flight plan. Percent change was calculated at $LOD_{high}$ as well as at intermediate concentrations. n=3 sensors plus a pHEMA-BMAP oxygen reference were tested at 37 C° and signal retention is reported as an average.

## 3.7 Long-term stability

Sensors were interrogated by periodic lactate challenges over 4 weeks to evaluate long term signal retention. On day 0, sensors (3 formulations, n=3 for each formulation, 2 sets, 18 sensors total) underwent flight plans ranging between 0 mg/dL-$LOD_{high}$. Sensors were stored at 37 C˚ in either PBS or 8 mg/dL lactate solution. PBS-stored samples were stored in 50 mL centrifuge tubes within a separate incubator. Lactate-exposed sensors were stored in a flow cell connected to an 8 mg/dL lactate reservoir under low flow conditions (1 mL/min); this accounts for lactate consumption and helps to maintain sensors in a steady lactate-concentrated environment. Thus, lactate-consumption concerns were mitigated, allowing for more rigorous experimentation. After 14 days and 28 days of storage, identical flight plans were administered. Afterwards, signal retention was calculated as seen in section 3.6; percent signal change was calculated as the difference in emission lifetimes at day 28 and day 0. Signal retention was calculated at $LOD_{high}$ as well as at intermediate concentrations.

# CHAPTER IV

# RESULTS AND DISCUSSION

## 4.1 Flow cell fabrication

A flow cell testing apparatus was designed and fabricated to evaluate sensor performance *in vitro*, Flow cells developed by past students interfaced with various lifetime measurement systems, yet none had been designed to work with the current instrument. Earlier flow cell iterations were typically made out of opaque materials with small windows to interrogate sensors, making it difficult to evaluate air bubble entrapment within the flow chamber. The proposed flow cell must transport lactate concentrated solution to the sensors while holding them in place. Further, flow cell material must mitigate light scattering effects to accurately assess sensor response. Thus, an optically clear flow cell which interfaces with the current bench-top system is needed.

To fabricate a flow cell, 7/16” thick optically clear cast acrylic (McMaster Carr, Elmhurst, IL) was used. From the acrylic two 8” x 3” rectangles were cut out using a table saw. An 11 mL flow chamber was milled into one of the acrylic pieces to define the path liquid takes through the cell. Initially, 3 wells were cut into the bottom of the chamber and distributed evenly along its axis. Later iterations contained 4 wells to include an additional oxygen sensor for baseline measurements. An o-ring groove was milled around the edge of the flow chamber to properly seal the cell. The superficial surface of the top piece contains two ports which deposit and retrieve liquid from the flow chamber, allowing for connection to the liquid pumping system. The inferior

surface boasts a 0.1” thick wall which seals along the inside surface of the flow chamber. Through holes for #10-32 metal screws were cut around the exterior edge of the flow cell. Drawings as well as an exploded view of the new flow cell design are shown in figure 4.1.

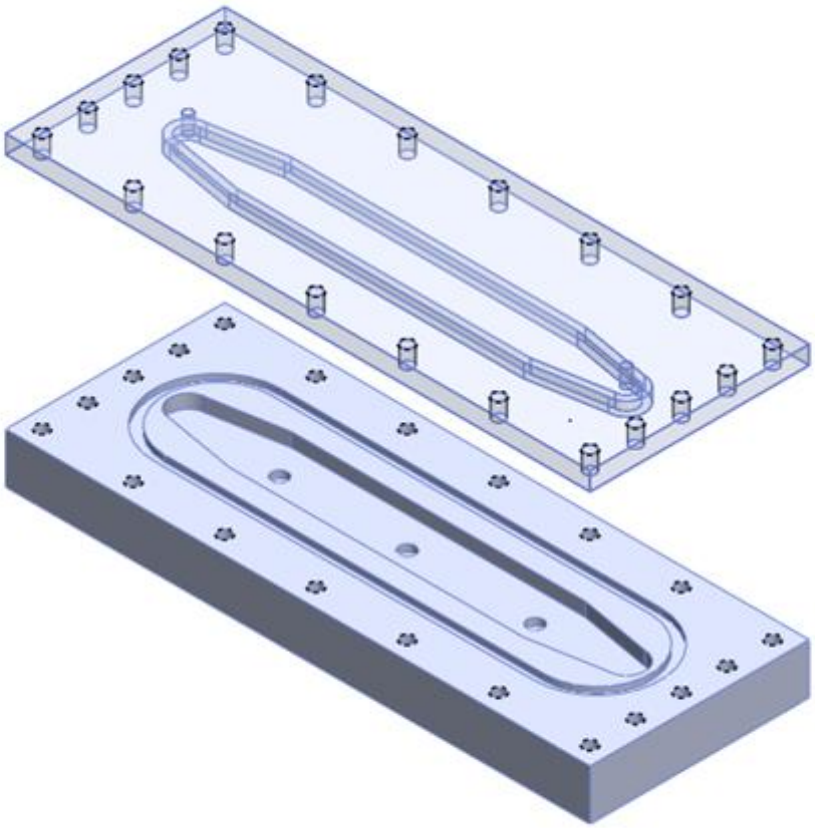

(**a**)

**Figure 4.1.** (**a**) Exploded view (**b**) & (**c**) drawings of top and bottom pieces

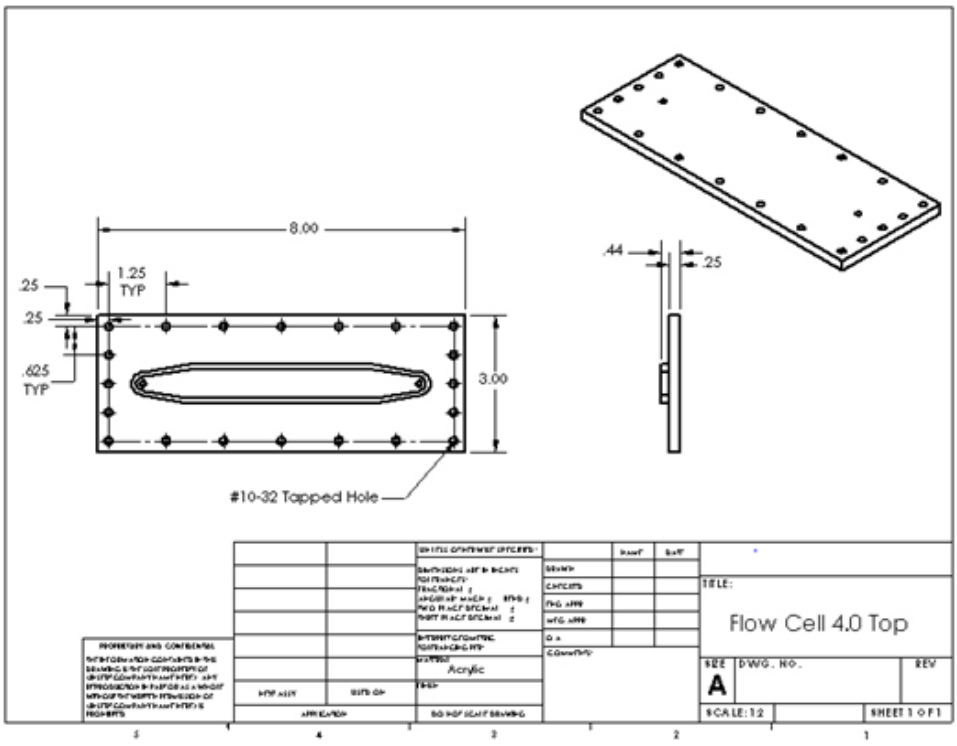


(**b**)

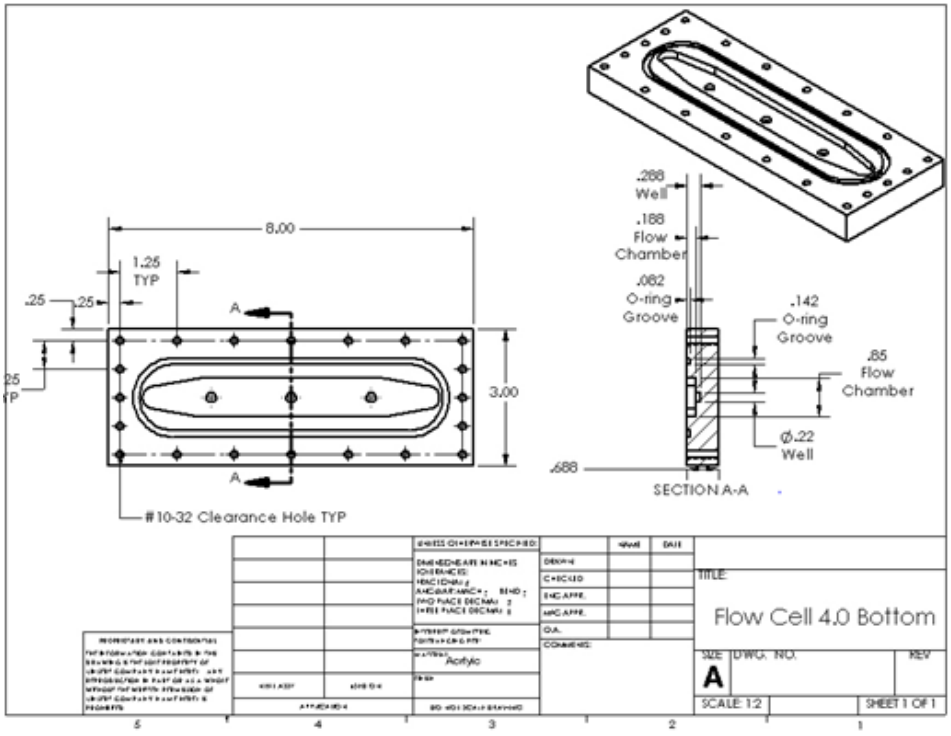


(**c**)

**Figure 4.1., Continued** (**a**) Exploded view (**b**) & (**c**) drawings of top and bottom pieces

Flow cell allows for quick experimental setup, permitting a high throughput testing environment. Designs were pre-programmed into CNC software; fabrication typically takes between 2-3 hours. After every lactate challenge, sensors are removed and flow cell is washed with ethanol and distilled water. O-rings, metal screws, and inlet/outlet ports are replaced periodically and flow cells are stored together when not in use.

## 4.2 Diffusion analysis

Figure 4.2a contains the measured permeate chamber lactate concentration for the three sensor types. Qualitatively, the increase in lactate transport through gels containing acrylamide is obvious. The calculated relative $D_L$ values for 75:25 pHEMA:pAam, 90:10 pHEMA:pAam, and pure pHEMA are $5.7\pm0.3*10^{-7}$ $cm^2/s$, $4.0\pm1.0*10^{-7}$ $cm^2/s$, and $3.1\pm1.6*10^{-7}$ $cm^2/s$, respectively. 90:10 pHEMA:pAam sensors display a small increase in lactate transport when compared to pure pHEMA, suggesting more pAam is needed in order to substantially effect swelling properties. For 75:25 pHEMA:pAam sensors, a ≈2 fold increase in lactate diffusion is seen relative to pHEMA sensors.

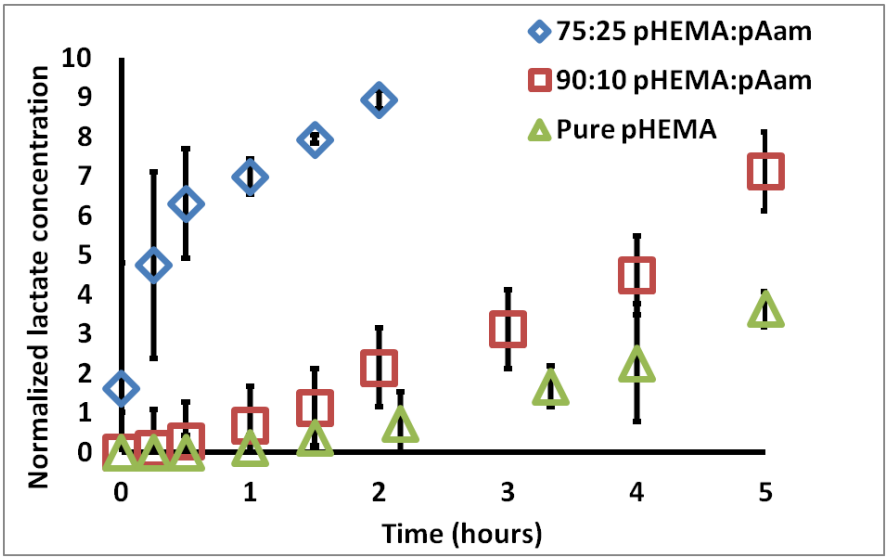


(**a**)

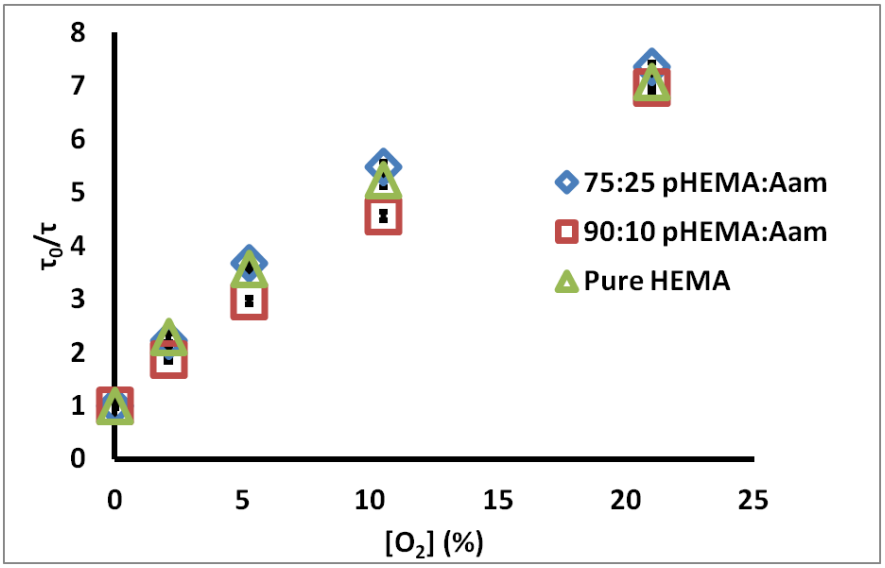


(**b**)

**Figure 4.2.** (**a**) Change of [lactate] in permeate chamber over time for three sensor types (**b**) Stern-Volmer plots for the same sensor types. Each set is an average of n=3 compositionally identical sensors; errors bars denote 95% confidence intervals (adapted from Andrus et al, 2015)[51b, 52]

Figure 4.2b contains $\tau_0/\tau$ vs. $[O_2]$ plots for each material tested. $K_{sv}$ values for 75:25 pHEMA:pAam, 90:10 pHEMA:pAam, and pure pHEMA are 0.29±0.003 $(\%\ O_2)^{-1}$,

$0.28\pm0.010$ (% $O_2$)$^{-1}$, and $0.28\pm0.002$ (% $O_2$)$^{-1}$, respectively. These $K_{sv}$ values match well with previous studies on similar materials[53]. Only the pure pHEMA and 75:25 formulations were statistically different at the 95% confidence level; this difference, while statistically significant, is only a matter of 3.6% increase in oxygen quenching. Thus, the effects on oxygen diffusion are minimal. This is not surprising, as $O_2$ is a very small, hydrophobic molecule with low solubility in water. Thus, transport may depend less on material cross-link density and more on the $O_2$ favorability of each material. It is most important to appreciate here that the changes in polymer formulation dramatically change lactate diffusion while minimally altering oxygen diffusion. Thus, this particular combination of polymers allows tuning of lactate diffusion almost completely independently from oxygen.

## 4.3 Sensor response

To determine characteristic sensor response, lactate challenges were administered. Figure 4.3a contains a representative real-time "flight plan" plot of the change in phosphorescent lifetime for three 75:25 pHEMA:pAam sensors to progressively higher lactate concentrations. The observed stepwise response is common to all formulations, regardless of composition. Most sensors matched well with others from the same batch, while a few cases (such as Channel 2 in Figure 3a) were significantly different in their response to intermediate lactate concentrations. All lactate sensors plateau at a maximum lifetime between 225 and 250 µs. A fourth trace represents the response of the oxygen sensor placed in the same channel, indicating the stable oxygen level observed in the steady state even during lactate challenges.

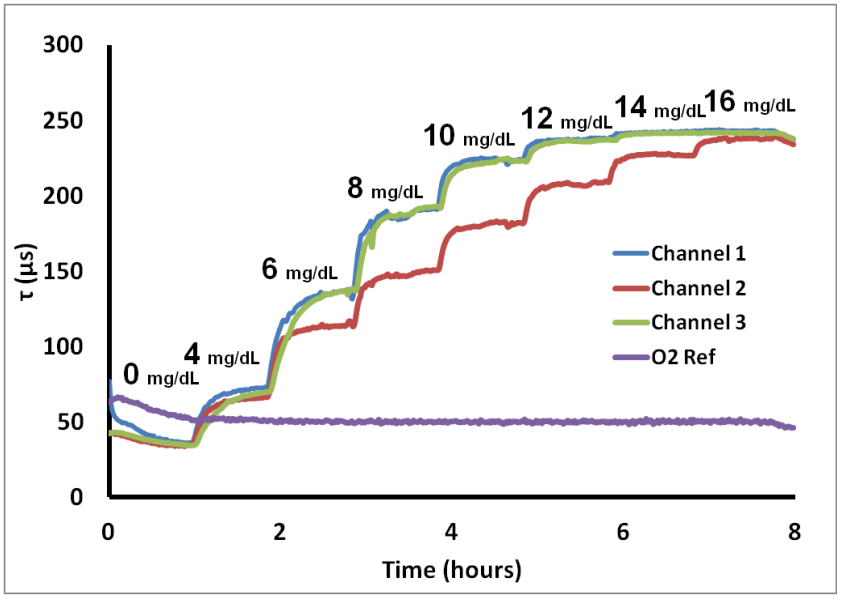


**(a)**

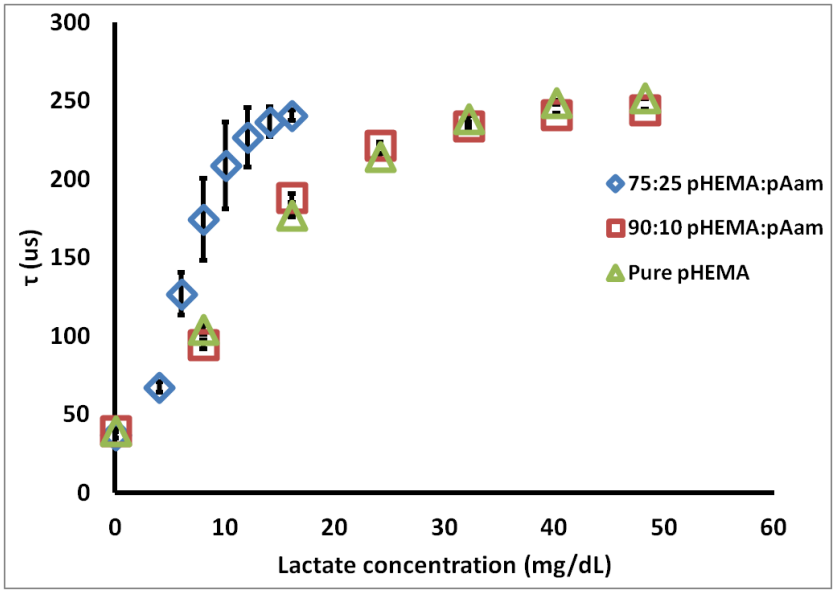


**(b)**

**Figure 4.3.** (**a**) 75:25 pHEMA:pAam lifetime response to lactate interrogation (**b**) calibration curves for three sensor types. Each calibration curve contains points representing the average phosphorescent lifetime; error bars denote the 95% confidence intervals for n=3 sensors (adapted from Andrus et al, 2015)[51b, 54]

Figure 4.3b shows calibration curves representing the steady-state response to lactate for sensors based on the three different hydrogel types. Several points can be made from these data. First, all of the formulations yield the same lifetime at zero lactate, again reinforcing that the oxygen diffusion properties are essentially the same for each case. It is also immediately apparent that the incorporation of 25% acrylamide dramatically shifts the sensor behavior from the other two cases. First, the sensitivity to lower lactate levels was increased, while the lactate concentration at which lifetime nears the maximum ($LOD_{high}$) was cut in approximately half. Furthermore, the amount of variability between sensors increased significantly, as indicated by the larger confidence intervals. This increased variability is primarily a result of batch heterogeneity, which was observed visually in preparing the hydrogels. The increased acrylamide content resulted in an obvious increase in gel phase separation/heterogeneity. Thus, sensors cut from the same initial hydrogel slab are more inconsistent in appearance. This apparent difference likely results in the changes in performance, which we attribute to variability in localized enzyme concentration and diffusion properties in the acrylamide-containing gels. This heterogeneity is less pronounced for the 90:10 copolymers.

Corresponding sensor figures of merit and diffusion metrics for the 75:25 pHEMA:pAam, 90:10 pHEMA:pAam, and pure pHEMA materials are reported in Table 1. These numbers quantitatively support the notion that increasing pAam precursor ratios are correlated to a decrease in range and a corresponding increase in sensitivity. This inverse relationship is explained by the properties of the two polymers. pAam is known to be significantly more hydrophilic than pHEMA due to polar amide groups present in

pAam's primary structure. In fact, pAam is able to take on ≈80% its weight in aqueous solution (compared to ≈37% for pHEMA)[55]. Higher concentrations of pAam lead to a more loosely cross-linked matrix, and therefore a more rapid diffusion profile, as is clearly seen from the measured relative lactate diffusion values. In contrast, however, previous reports cited a much larger increase of diffusion when comparing pAam to pHEMA; diffusion of small molecules has been shown to be several orders of magnitude higher in pAam when compared to pure pHEMA[28]. Thus, the copolymer system retains a strong influence of the pHEMA even with 25% pAam.

This change in diffusivity alters kinetics of immobilized LOx and the resulting oxygen consumption profiles. Increased swelling allows local lactate and $O_2$ molecules to interact more readily with LOx active sites, encouraging rapid enzyme saturation. As more $O_2$ is consumed, BMAP is quenched less and therefore emits with a longer average lifetime. Thus, the optical saturation is reached at lower bulk lactate concentrations. Higher pAam concentration increases enzyme-substrate contact, effectively lowering usable range of the device.

An interesting note is that $D_L$ values scale well with sensitivity metrics. Addition of only 10% pAam does little to increase lactate diffusion (and therefore sensitivity). pAam is much more hydrophilic than pHEMA, but is needed in higher ratios to significantly affect gel micro-structure. Both sensitivity and $D_L$ metrics for the 75:25 pHEMA:pAam sensor are double what is seen in pure pHEMA gels, indicating promise for high measurement precision within a normal lactate range.

Total change in lifetime, Δτ, was similar for materials tested. Sensors all started with similar baseline τ; this means Δτ is mostly dependent on τ at enzyme saturation. A small statistical difference between pure pHEMA and 75:25 pHEMA:pAam sensors is seen, ≈4 μs; Δτ for 90:10 pHEMA gels overlap with the other two materials.

Calculated response time is not statistically different between the materials. All materials were able to achieve a stable optical response within a 20-minute window after introducing the step change in lactate level. This is similar to response times for current electrochemical-based sensors and is considered adequate to effectively monitor fluctuations in systemic conditions.

**Table 1.** Compiled sensor metrics, values are average of n=3 sensors ± 95% confidence intervals (adapted from Andrus et al, 2015)[51b, 56]

| **Monomers** | **75:25 pHEMA:pAam** | **90:10 pHEMA:pAam** | **Pure pHEMA** |
|---|---|---|---|
| **Sensitivity [μs*dL/mg]** | 20.0±2.3 | 9.2±1.5 | 8.5±2.2 |
| **Range [mg/dL]** | 1.1-12.7 | 0.7-35.0 | 0.4-38.2 |
| **$\Delta\tau$ [μs]** | 203.9±1.5 | 204.6±4.3 | 212.0±4.0 |
| **Response time [min]** | 19.0±2.9 | 16.4±1.7 | 15.2±1.2 |
| **$D_L$ [$cm^2/s$]*$10^{-7}$** | 5.7±0.3 | 4.0±0.9 | 3.1±1.6 |
| **$\tau_0$ [μs]** | 251.8±5.1 | 259.9±8.9 | 290.0±7.3 |
| **$K_{sv}$ [$\%^{-1}$ $O_2$]*$10^{-2}$** | 29.4±0.3 | 28.0±1.2 | 27.7±0.2 |
| **Signal retention @ $LOD_{high}$ [%]** | | | |
| *after 20 cycles* | 73.11±14.9 | 81.0±10.6 | 69.9±4.9 |
| *4 weeks, PBS storage* | 18.4±4.0 | 63.3±10.2 | 59.7±10.7 |
| *4 weeks, lactate storage* | 3.6 ±3.9 | 7.0±3.7 | 3.3±2.1 |

## 4.4 Acute stability

To evaluate acute signal reduction in response to lactate, sensors were exposed to 20 consecutive lactate challenges. Lifetime values at 5, 10, and 20 lactate challenges were compared against initial flight plan lifetimes for freshly prepared sensors. Signal retention was calculated as a metric of the change in τ after repeated lactate flight plans. The relative difference of τ at cycle (flight plan) 20 to τ at cycle 1 is described in equation 4.1.

$$Signal\ retention\ (\%) = \left[\frac{\left(\tau_{cycle\ x20} - \tau_{cycle\ 01}\right)}{\tau_{cycle\ x1} - \tau_{cycle\ 01}}\right] * 100$$

**Equation 4.1.** Signal retention calculation

where $\tau_{cycle\ x20}$ is the emission lifetime at cycle 20, $\tau_{cycle\ x1}$ is lifetime for same concentration on the initial cycle, and $\tau_{cycle\ 01}$ is the baseline $\tau$ recorded at 0 mg/dl lactate on cycle 1.

Figure 4.4a contains representative data from the 90:10 pHEMA:pAam materials, indicating how the measured τ values at each lactate concentration changed over 20 cycles. Figure 4.4b is a summary of the signal retention over 20 cycles for all three sensor types. For 75:25 pHEMA:Aam sensors, signal retention of 78.1±9.0%, 76.1±18.4%, 73.1±14.9% is seen at 1/3 $LOD_{high}$, 2/3 $LOD_{high}$, and $LOD_{high}$, respectively. For 90:10 pHEMA:pAam sensors, signal retention of 85.5±20.8%, 80.6±16.5%, 81.0±10.6% is seen at 1/3 $LOD_{high}$, 2/3 $LOD_{high}$, and $LOD_{high}$, respectively. Finally, for

pure pHEMA sensors, signal retention of 34.9±11.8%. 56.1±8.0%, 69.9±4.9%, is seen at 1/3 $LOD_{high}$, 2/3 $LOD_{high}$, and $LOD_{high}$, respectively.

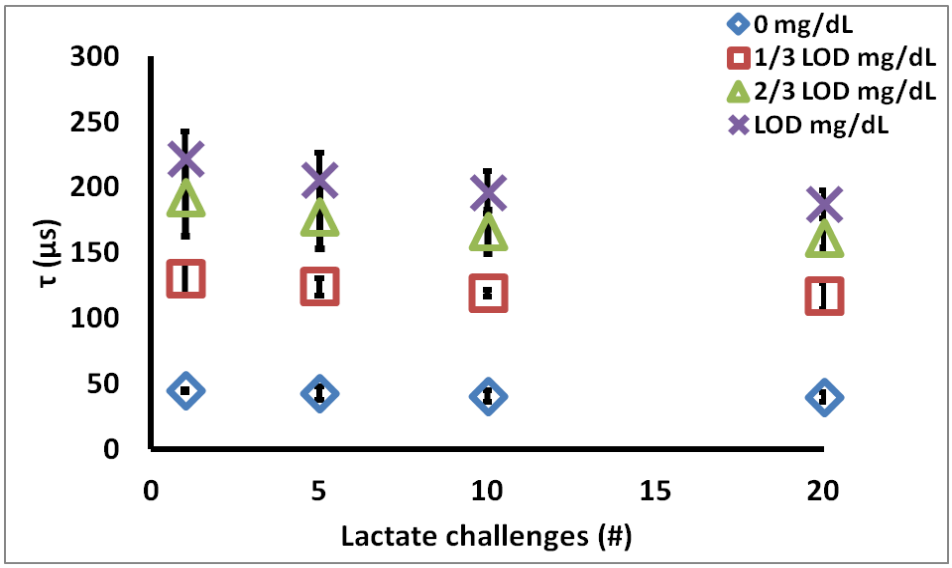


**(a)**

**Figure 4.4.** (**a**) 90:10 pHEMA:pAam signal retention over 20 cycles (**b**) % retention of first cycle signal (**c**) % retention of fifth cycle signal, Markers indicate average values, and error bars represent 95% confidence intervals between measured signal retention for n=3 sensors (adapted from Andrus et al, 2015)[51b, 57]

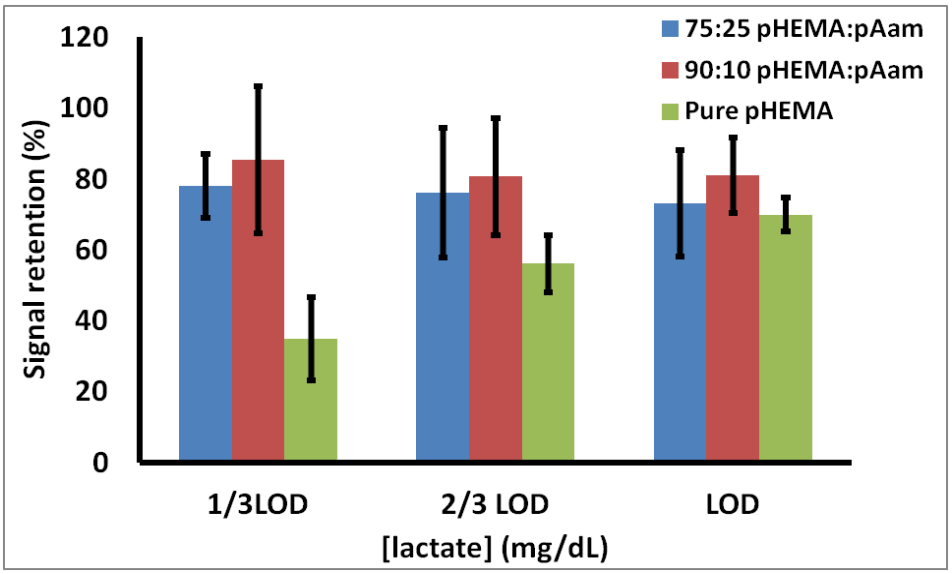


**(b)**

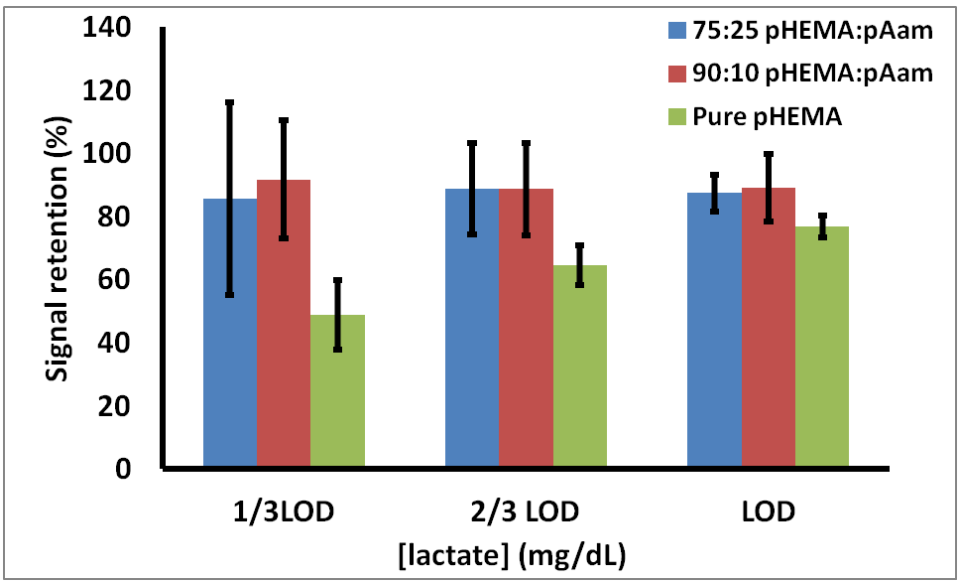


**(c)**

**Figure 4.4., Continued** (**a**) 90:10 pHEMA:pAam signal retention over 20 cycles (**b**) % retention of first cycle signal (**c**) % retention of fifth cycle signal, Markers indicate average values, and error bars represent 95% confidence intervals between measured signal retention for n=3 sensors (adapted from Andrus et al, 2015)[51b, 57]

Investigation of acute signal loss reveals an initial reduction in emission lifetime before a pseudo-stable response is reached, as there is no statistical change in $\tau$ after the $5^{th}$ exposure cycle (Figure 4.4a). This "break-in" could be due to leaching of LOx not covalently bound to the hydrogel. A protein leaching study was performed on freshly-prepared sensors using a colorimetric enzyme assay. n=3 sensors were stirred in 1 mL DI water, and results indicates no active enzyme present in solution above 10 ng/mL (data not shown). It should be noted that this leaching study indicates no loss of active enzyme and does not account for loss of denatured LOx. Nonetheless, chemical and mechanical stresses induced on enzyme during polymerization and swelling during equilibration are likely culprits for the apparent loss in sensitivity. Partially unstable protein moieties quickly denature within first lactate flight plan, leaving remaining LOx to function properly. Figure 4.4c shows signal retention at $LOD_{high}$ between cycles 5-20. After an initial loss in activity, pAam-containing materials maintained a stable response, with no statistical difference from the $5^{th}$ cycle response to the $20^{th}$ cycle at any of the tested lactate concentrations.

These data suggest a positive relationship between sensor stability and increasing pAam concentration. Both 75:25 pHEMA:pAam and 90:10 pHEMA:pAam materials experienced statistically similar signal retention throughout the study, while pure pHEMA formulations displayed higher levels of LOx activity loss (about 50-70% retention between cycles 5-20). It follows that gels containing some acrylamide are better suited for retaining LOx activity, most likely due to the hydrophilic nature of

pAam that yields an encapsulation more consistent with the enzymes' native environment.

Aside from leaching, chemical and mechanical denaturation issues, none of which were observed in our studies, enzyme activity is the primary issue for sensor stability. It is difficult to quantify enzyme activity within a semisolid medium. Furthermore, it is important to appreciate that, upon hydrogel immobilization, the kinetics of LOx no longer exclusively depend on lactate concentration. The LOx-polymer interface restricts transport, making substrate less available as when in solution. This means that the hydrogel microstructure will directly affect the rate of lactate delivery to the enzyme; this system requires normalizing conditions for direct comparison. Since each material has a different calculated $LOD_{high}$, we chose to expose sensors to normalized concentrations relative to this upper limit during the experiment; this resulted in different absolute bulk lactate concentrations but effectively the same lactate flux. Although $LOD_{high}$ was used in an attempt to normalize data, we recognize that dissimilar lactate challenges may provide for variable concentrations of substrate near immobilized LOx and therefore different reaction rates.

## 4.5 Long-term stability

Figure 4.5a is a summary of the signal retention over 2 weeks for all three sensor types. For 75:25 pHEMA:Aam sensors stored in PBS, signal retention of 96.0±35.3%, 78.6±17.0%, 82.8±6.1% is seen at 1/3 $LOD_{high}$, 2/3 $LOD_{high}$, and $LOD_{high}$, respectively. For 75:25 pHEMA:Aam sensors stored in lactate, signal retention of 10.9±12.0%, 6.6±4.5%, 6.3 ±3.7% is seen at 1/3 $LOD_{high}$, 2/3 $LOD_{high}$, and $LOD_{high}$, respectively. For

90:10 pHEMA:pAam sensors stored in PBS, signal retention of 71.0±26.7%, 67.6±17.1%, 83.3±5.8% is seen at 1/3 $LOD_{high}$, 2/3 $LOD_{high}$, and $LOD_{high}$, respectively. For 90:10 pHEMA:pAam sensors stored in lactate, signal retention of 11.2±6.3%, 10.7±1.0%, 19.5±1.0% is seen at 1/3 $LOD_{high}$, 2/3 $LOD_{high}$, and $LOD_{high}$, respectively. For pure pHEMA sensors stored in PBS, signal retention of 82.8±41.4%, 99.7±8.0%, 97.9±1.0% is seen at 1/3 $LOD_{high}$, 2/3 $LOD_{high}$, and $LOD_{high}$, respectively. For pure pHEMA sensors stored in lactate, signal retention of 8.7±5.7%, 11.4±1.7%, 24.0±2.6% is seen at 1/3 $LOD_{high}$, 2/3 $LOD_{high}$, and $LOD_{high}$, respectively.

Figure 4.5b is a summary of the signal retention over 4 weeks for all three sensor types. For 75:25 pHEMA:Aam sensors stored in PBS, signal retention of 52.3±13.0%, 22.7±5.9%, 18.4±4.0% is seen at 1/3 $LOD_{high}$, 2/3 $LOD_{high}$, and $LOD_{high}$, respectively. For 75:25 pHEMA:Aam sensors stored in lactate, signal retention of 8.8±10.1%, 4.8±5.9%, 3.6 ±3.9% is seen at 1/3 $LOD_{high}$, 2/3 $LOD_{high}$, and $LOD_{high}$, respectively. For 90:10 pHEMA:pAam sensors stored in PBS, signal retention of 25.8±8.2%, 45.0±12.7%, 63.3±10.2% is seen at 1/3 $LOD_{high}$, 2/3 $LOD_{high}$, and $LOD_{high}$, respectively. For 90:10 pHEMA:pAam sensors stored in lactate, signal retention of 20.0±12.6%, 7.6±4.8%, 7.0±3.7% is seen at 1/3 $LOD_{high}$, 2/3 $LOD_{high}$, and $LOD_{high}$, respectively. For pure pHEMA sensors stored in PBS, signal retention of 25.4±4.5%, 42.7±13.5%, 59.7±10.7% is seen at 1/3 $LOD_{high}$, 2/3 $LOD_{high}$, and $LOD_{high}$, respectively. For pure pHEMA sensors stored in lactate, signal retention of 1.8±4.2%, 2.1±2.0%, 3.3±2.1% is seen at 1/3 $LOD_{high}$, 2/3 $LOD_{high}$, and $LOD_{high}$, respectively.

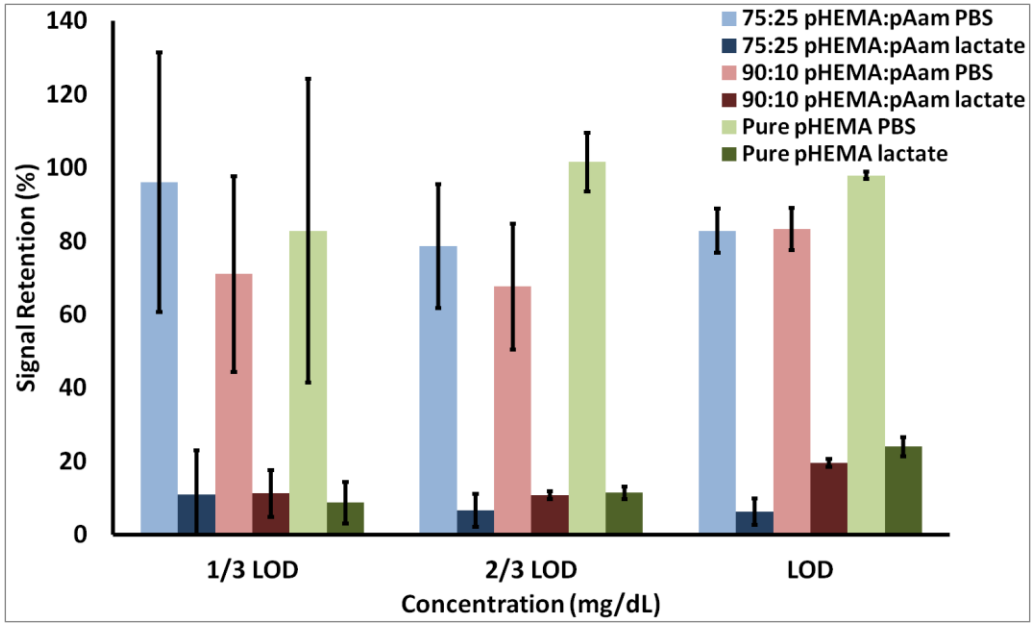


(**a**)

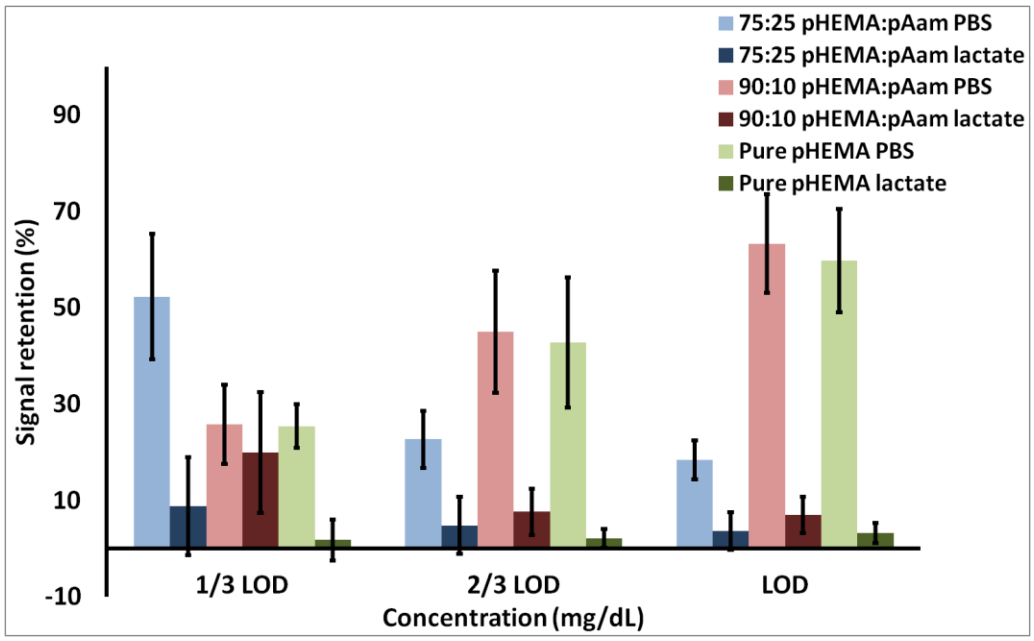


(**b**)

**Figure 4.5.** (**a**) % signal retention after 2 weeks (**b**) signal retention after 4 weeks, Markers indicate average values, and error bars represent 95% confidence intervals between measured signal retention for n=3 sensors

PBS-stored sensors typically retain sensitivity better than sensors stored in 8 mg/dL lactate, although signal loss is still significant throughout. At high lactate concentrations, both 90:10 pHEMA:pAam and pure pHEMA sensors stored in PBS maintain sensitivity better than 75:25 pHEMA:pAam. This is surprising, since acute degradation studies suggest materials with higher pAam content to be more suitable for enzyme immobilization. It follows that short term signal retention is higher in pAam-containing gels, although over 2 and 4 weeks the largely pHEMA gels perform better, indicating LOx immobilized in the pure pHEMA and 90:10 pHEMA:pAam materials resists thermal deactivation better than LOx immobilized in the more loosely cross-linked 75:25 pHEMA:pAam matrix. Similar signal retention is observed between pure pHEMA and 90:10 pHEMA:pAam materials, while 75:25 pHEMA:pAam materials display a significantly different signal retention profile, again suggesting that incorporation of only 10% pAam does little to affect sensor response.

While PBS-stored sensors exhibit some signal change after 4 weeks of storage, lactate-stored sensors display minimal sensitivity after 2 weeks. Week 2 and 4 lactate-storage data indicates significant deactivation, suggesting poor stability under physiological-like conditions. An interesting note is that signal retention trends with pHEMA content for lactate-stored sensors at $LOD_{high}$. This may be explained by the relative lactate flux through each material. pAam-containing sensors display higher $D_L$ values, thus storage in 8 mg/dL lactate solution may result in increased catalytic activity when compared to pure pHEMA sensors. Increased catalysis may lead to more rapid enzyme deactivation, thus decreasing sensor stability.

Data suggests sensors may resist thermal deactivation (from PBS-storage results), yet high temperatures coupled with a catalytically active environment (lactate-storage) yields substantial signal loss. Although 8 mg/dL lactate is within the physiologically relevant range of concentrations, it may be a worst case scenario. In future studies, lower lactate concentrations should be considered.

# CHAPTER V

# CONCLUSIONS AND FUTURE WORK

## 5.1 Sensor characterization

*In vitro* characterization of a novel biosensor designed for lactate detection has been described. As far as we know, this study presents an implantable, phosphorescent lactate sensor never-before-seen in previous literature. An enzyme-oxygen, phosphor sensing chemistry was immobilized within three different co-polymer formulations, allowing for tunable macro sensor characteristics by controlling substrate diffusion through careful co-polymer selection. To demonstrate the diffusion-controlled nature of this platform, bulk transport properties of both lactate and oxygen were assessed; results indicate a positive relationship between diffusivity and sensitivity. This matched expectations based on known hydrophilicity differences between the pHEMA and pAam materials studied, though the magnitude of the gains in oxygen diffusivity were surprisingly low. Furthermore, this tuning in response properties was possible by adjusting lactate diffusion with minimal effect on oxygen diffusion and phosphor sensitivity to oxygen.

While the hydrogel composition effects transport properties, there was also an apparent change in acute stability that favors the incorporation of at least some acrylamide. Interestingly, sensor stability to repeated lactate challenges does not directly

correlate with the diffusion properties studied herein. Results from 2 and 4 week stability evaluation indicate substantial loss of lactate sensitivity for all materials tested.

## 5.2 Low $O_2$ testing

### 5.2.1 Low $O_2$ testing setup

It is well known that oxygen concentrations in subcutaneous tissue are significantly lower than ambient concentrations[58]. Therefore, sensors were interrogated by lactate challenges at low oxygen to accurately assess *in vivo* capabilities. To evacuate oxygen, a Systec® Prep/Semi-Prep Scale degassing chamber (Biotech AB, Onsala, SE) and a Systec® ZHCR® vacuum pump were incorporated into the current bench-top testing system (figure 3.1). Degasser-vacuum pump combination is installed in-line between the VICI liquid pumps and the flow cell. Solution is flowed through the degassing chamber, thus removing dissolved gas prior to sensor exposure. Initially, sensors were subjected to pure PBS and ambient oxygen for 1 hour. Next, the vacuum pump was turned on and ran for 2 hours prior to lactate challenge, allowing for sensor stabilization at low oxygen. Afterwards, lactate challenges were administered as described in section 3.3, albeit at lower lactate concentrations. A microcontroller configured to the pump maintained vacuum pressure at 80 mmHg. Sensors were subjected to each lactate concentration for 1 hour at a flow rate of 4 mL/min and phosphorescent lifetimes were monitored using the BEACON instrument. Data analysis was performed following procedure outlined in section 3.4. All lactate challenges were performed at 37 C°.

### 5.2.2 Low $O_2$ testing results

To determine characteristic sensor response at low oxygen, lactate challenges were administered. Figure 5.1a contains a representative real-time lactate flight plan of n=3 pure pHEMA sensors. Figure 5.1b contains lactate calibration curves at low oxygen for all materials. Figure 5.1c contains these calibrations juxtaposed against calibrations of same sensors at ambient oxygen.

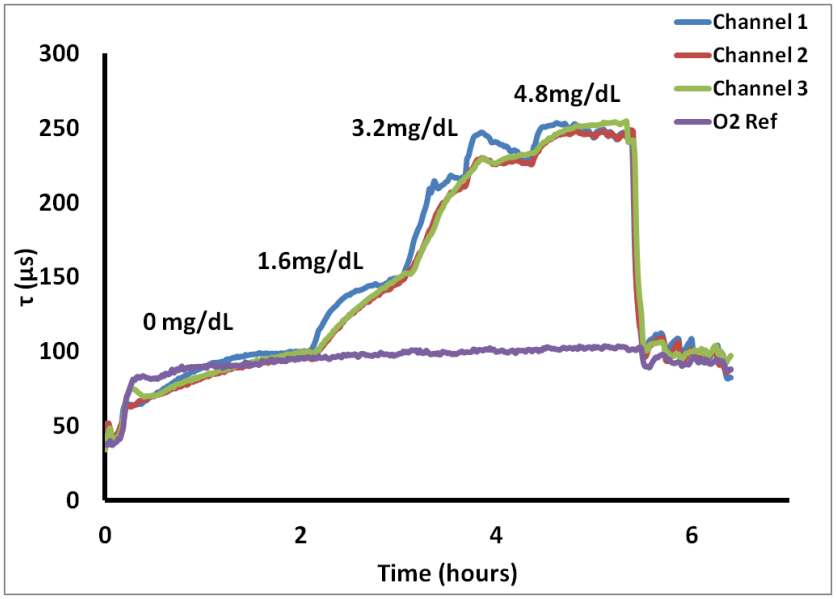


**(a)**

**Figure 5.1.** (**a**) Pure pHEMA lifetime response to lactate interrogation at low oxygen (**b**) calibration curves for three sensor types at low oxygen. Each calibration curve contains points representing the average phosphorescent lifetime; error bars denote the 95% confidence intervals for n=3 sensors (**c**) calibration curves for three sensor types at low oxygen and ambient oxygen

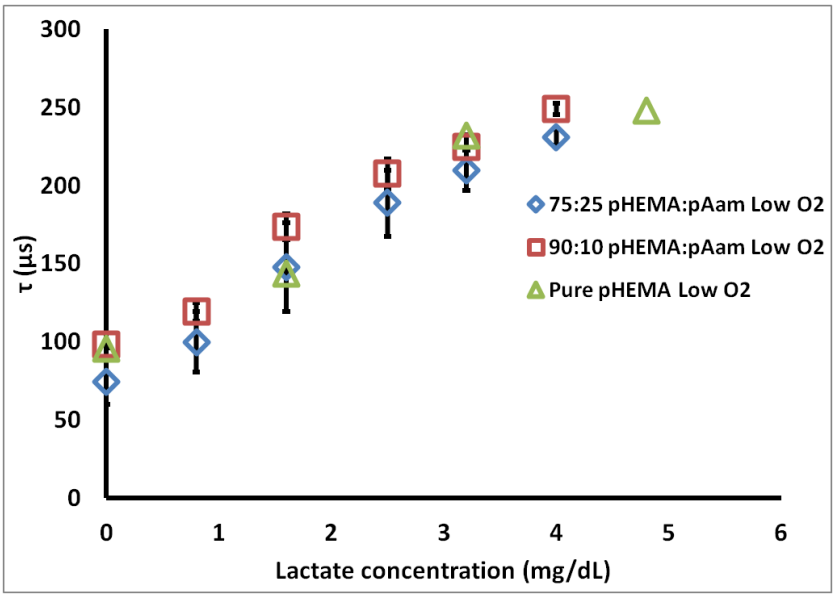


(**b**)

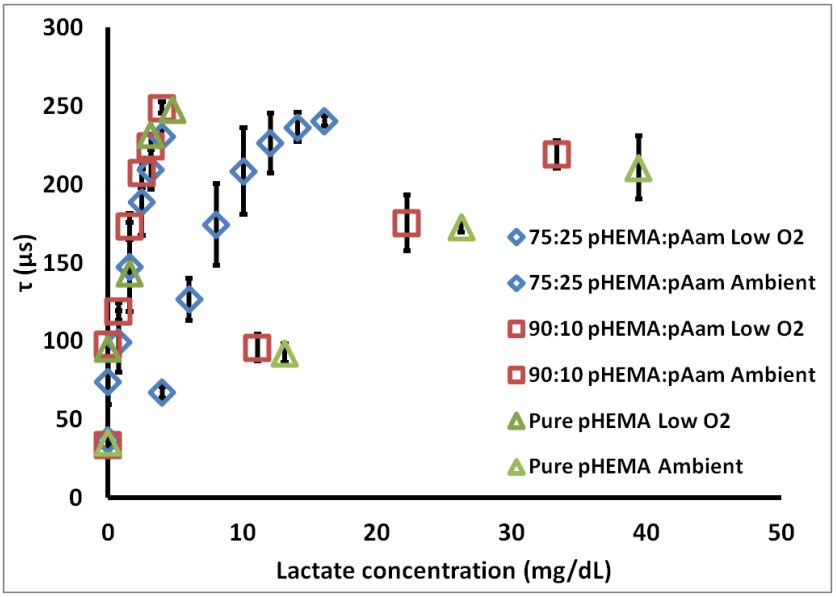


(**c**)

**Figure 5.1., Continued** (**a**) Pure pHEMA lifetime response to lactate interrogation at low oxygen (**b**) calibration curves for three sensor types at low oxygen. Each calibration curve contains points representing the average phosphorescent lifetime; error bars denote the 95% confidence intervals for n=3 sensors (**c**) calibration curves for three sensor types at low oxygen and ambient oxygen

Corresponding sensor performance metrics at low $O_2$ for the 75:25 pHEMA:pAam, 90:10 pHEMA:pAam, and pure pHEMA materials are reported in Table 2. Low oxygen testing revealed a decrease in analytical range for all materials tested; analytical range is reduced (≈3.5x reduction for 75:25 pHEMA:pAam sensors, ≈9x reduction for 90:10 pHEMA:pAam sensors, and ≈11x reduction for pure pHEMA sensors) when compared sensor response at ambient oxygen. 80 mmHg vacuum pressure on the testing system at 0 mg/dL lactate results in baseline lifetimes $\tau$≈100 µs for 90:10 pHEMA:pAam and pure pHEMA materials; this matches well with baseline lifetimes observed *in vivo* for similar pHEMA-BMAP oxygen sensors (data not shown). However, baseline lifetimes (0 mg/dL lactate) for 75:25 pHEMA:pAam sensors are $\tau$≈75 µs, indicating addition of pAam may allow higher levels of available oxygen in these materials. These short baseline lifetimes indicate pAam-containing materials may possess higher $\Delta\tau$ (and thus broader lactate sensitivity at low oxygen), although 75:25 pHEMA:pAam sensors display rapid saturation upon lactate exposure as is seen in pure pHEMA sensors. Data suggests pAam may increase oxygen permeability, yet the increase in lactate transport through pAam-containing gels ultimately leads to rapid saturation.

**Table 2.** Compiled sensor metrics at low $O_2$, values are average of n=3 sensors ± 95% confidence intervals

| **Monomers** | **75:25 pHEMA:pAam** | **90:10 pHEMA:pAam** | **Pure pHEMA** |
|---|---|---|---|
| **Sensitivity [µs*dL/mg]** | 47.1±4.7 | 46.1±3.5 | 42.6±1.1 |
| **Range [mg/dL]** | 0.3-3.4 | 0.5-3.9 | 0.6-3.5 |
| **$\Delta\tau$ [µs]** | 156.6±11.0 | 151.2±5.0 | 152.6±4.0 |

## 5.3 Limitations and future work

### 5.3.1 Low $O_2$

Analytical range is significantly reduced during low oxygen testing; these results indicate oxygen availability may be the limiting factor *in vivo.* It is therefore likely that alternate materials with better oxygen transport may be better suited for long-term functionality. One potential solution is to further decrease lactate diffusion. Lower $D_L$ values correspond to less lactate/oxygen consumption, which could provide sensitivity over a broader range. This approach may require the use of materials other than pHEMA and pAam. Although other hydrogel materials may further restrict of lactate transport, they may also decrease oxygen permeability; this would be counter-productive, as data indicates oxygen availability to be a limiting factor. An ideal material would encourage oxygen transport while exhibiting $D_L$ values similar to sensors tested here.

Results indicate further work is needed to develop sensors with adequate sensitivity at low oxygen. Certain siloxane-containing monomers are characterized by high oxygen permeability. Immobilization in such materials would increase oxygen availability to sensing chemistry. In theory, improved *in vivo* functionality may be achieved if pore size can be tuned to adequately restrict lactate transport.

Another approach is to decrease LOx concentration in current and future sensor iterations. Reduction of LOx decreases local oxygen consumption, potentially providing

sensitivity at higher bulk lactate concentrations. An intensive panel containing siloxane-based materials with varying concentrations of immobilized enzyme is likely needed to fabricate a sensor with appropriate sensitivity *in vivo*.

### 5.3.2 Sensor stability

Sensors studied here display signal loss in both acute- and long-term studies, indicated by enzyme deactivation; this suggests enzyme-modification techniques may be applied prior to immobilization to enhance catalytic stability. Work by Ritter et al details glycosylation site-targeted attachment of poly(ethylene glycol) (PEG) chains to GOx. PEG-GOx displays higher resistance to deactivation when compared to native GOx[59]. Similarly, unpublished work by our group indicates electrostatic attachment of poly(ethylenimine) (PEI) to GOx improves thermal and operational stability. While these studies primarily focus on GOx modification, they could, in principle, also be applied to LOx.

### 5.3.3 Fabrication repeatability

Sensors cut from the same gel display slightly different response profiles. Increasing pAam content seems to exacerbate batch-to-batch variability. This could be due to heterogeneity seen in pAam-containing gels; a result of disparate co-solvents (DMSO for Aam, aqueous buffer for LOx-catalase). Phase separation pre-polymerization may be indicative of heterogeneous distribution of sensing chemistry. Repeatability is essential and variable enzyme concentrations between sensors may lead to disparate sensitivities. Clearly, work is needed to determine extent of phase separation

and subsequent enzyme aggregation. An enzyme modification technique that alters surface hydrophilicity as well as stabilizes catalytic activity would be ideal. Modified LOx dissolved in a mild organic solvent prior to polymerization may provide for better mixing of precursor solution. Alternatively, it may be possible to reduce heterogeneity by using different co-solvents altogether. There may exist a "happy medium" between aqueous and organic solvents which would maintain adequate enzyme stability while also providing for a well mixed precursor solution.

### 5.3.4 Testing system

The flow through system described here maintains a flow rate of 4 mL/min throughout each flight plan. This allows for autonomous control over lactate concentrations exposed to sensing materials, however inherent convective transport is also present. Implanted sensors are exposed to diffusion only; convection is not an issue in subcutaneous tissue. There may be changes in response to lactate within a flow through system caused by convection. Nonetheless, a flow through system was deemed necessary to interrogate materials and provides preliminary analysis of tunable sensing platform. Currently work is being done to immobilize sensors in highly diffusive polymers (e.g. PEG) within the flow cell prior to testing. This would provide diffusion-only transport to the sensor surface. PEG may reduce diffusion rates, creating another variable when analyzing data. Ideally, sensors would be immobilized in a PEG medium with lactate and oxygen diffusion characteristics similar to water, thus eliminating convection while maintaining comparable diffusion rates.

## 5.4 Multiple analyte detection

This study highlights the general applicability of the enzyme-oxygen phosphor-hydrogel platform for analyte sensing as it is a modification of a previous glucose sensor. Substitution of analyte-specific enzymes within similar hydrogel materials allows for sensitivity over a physiologically relevant lactate range. Again, the high degree of control over small molecule diffusion (and thus macro sensor characteristics) demonstrates how materials can modulate sensor response over a wide range. This platform, in principle, may be used for sensing of other biochemistries such as cholesterol, pyruvate, alcohol, thiamine, xanthine, and choline, among others. Future studies will investigate alternative-analyte detection towards the goal of multi-analyte sensing within a single sensor.

REFERENCES


1. (a) Gaster, R. S.; Hall, D. A.; Wang, S. X., nanoLAB: An ultraportable, handheld diagnostic laboratory for global health. *Lab on a Chip* **2011,** *11* (5), 950-956; (b) Ayub, M.; Ivanov, A.; Instuli, E.; Cecchini, M.; Chansin, G.; McGilvery, C.; Hong, J.; Baldwin, G.; McComb, D.; Edel, J. B.; Albrecht, T., Nanopore/electrode structures for single-molecule biosensing. *Electrochimica Acta* **2010,** *55* (27), 8237-8243.

2. Nathan, D. M., Long-Term Complications of Diabetes Mellitus. *New England Journal of Medicine* **1993,** *328* (23), 1676-1685.

3. (a) Department of Health and Human Services: Center for Disease Control and Prevention. **2011**; (b) Wild, S.; Roglic, G.; Green, A.; Sicree, R.; King, H., Global Prevalence of Diabetes: Estimates for the year 2000 and projections for 2030. *Diabetes Care* **2004,** *27* (5), 1047-1053.

4. Sowers, J. R.; Epstein, M.; Frohlich, E. D., Diabetes, Hypertension, and Cardiovascular Disease: An Update. *Hypertension* **2001,** *37* (4), 1053-1059.

5. Cryer, P. E., Death during Intensive Glycemic Therapy of Diabetes: Mechanisms and Implications. *The American Journal of Medicine* **2011,** *124* (11), 993-996.

6. Puente, E. C.; Silverstein, J.; Bree, A. J.; Musikantow, D. R.; Wozniak, D. F.; Maloney, S.; Daphna-Iken, D.; Fisher, S. J., Recurrent Moderate Hypoglycemia Ameliorates Brain Damage and Cognitive Dysfunction Induced by Severe Hypoglycemia. *Diabetes* **2010,** *59* (4), 1055-1062.

7. Patterson, C. C.; Dahlquist, G.; Harjutsalo, V.; Joner, G.; Feltbower, R. G.; Svensson, J.; Schober, E.; Gyürüs, E.; Castell, C.; Urbonaité, B.; Rosenbauer, J.; Iotova, V.; Thorsson, A. V.; Soltész, G., Early mortality in EURODIAB population-based cohorts of type 1 diabetes diagnosed in childhood since 1989. *Diabetologia* **2007,** *50* (12), 2439-2442.

8. Feltbower, R. G.; Bodansky, H. J.; Patterson, C. C.; Parslow, R. C.; Stephenson, C. R.; Reynolds, C.; McKinney, P. A., Acute Complications and Drug Misuse Are

Important Causes of Death for Children and Young Adults With Type 1 Diabetes: Results from the Yorkshire Register of Diabetes in Children and Young Adults. *Diabetes Care* **2008,** *31* (5), 922-926.

9. Skrivarhaug, T.; Bangstad, H. J.; Stene, L. C.; Sandvik, L.; Hanssen, K. F.; Joner, G., Long-term mortality in a nationwide cohort of childhood-onset type 1 diabetic patients in Norway. *Diabetologia* **2006,** *49* (2), 298-305.

10. The Effect of Intensive Treatment of Diabetes on the Development and Progression of Long-Term Complications in Insulin-Dependent Diabetes Mellitus. *New England Journal of Medicine* **1993,** *329* (14), 977-986.

11. White, N. J., Lactate trumps blood pressure for trauma triage. *Science Translational Medicine* **2015,** *7* (278), 278ec43.

12. CADY, L. D. J.; WEIL, M. H.; AFIFI, A. A.; MICHAELS, S. F.; LIU, V. Y.; SHUBIN, H., Quantization of severity of critical illness with special reference to blood lactate. *Critical Care Medicine* **1973,** *1* (2), 75-80.

13. Westerblad, H.; Allen, D. G.; Lännergren, J., *Muscle Fatigue: Lactic Acid or Inorganic Phosphate the Major Cause?* 2002; Vol. 17, p 17-21.

14. Nguyen, H. B.; Rivers, E. P.; Knoblich, B. P.; Jacobsen, G.; Muzzin, A.; Ressler, J. A.; Tomlanovich, M. C., Early lactate clearance is associated with improved outcome in severe sepsis and septic shock. *Crit Care Med* **2004,** *32* (8), 1637-42.

15. Matsushita, K.; Williams, E. K.; Mongraw-Chaffin, M. L.; Coresh, J.; Schmidt, M. I.; Brancati, F. L.; Hoogeveen, R. C.; Ballantyne, C. M.; Young, J. H., The Association of Plasma Lactate With Incident Cardiovascular Outcomes: The ARIC Study. *American Journal of Epidemiology* **2013,** *178* (3), 401-409.

16. Nakao, T., Impaired lactate production by skeletal muscle with anaerobic exercise in patients with chronic renal failure. A possible consequence of defective glycolysis in skeletal muscle. *Nephron* **1982,** *31* (2), 111-115.

17. Heiss, W.-D., The ischemic penumbra: how does tissue injury evolve? *Annals of the New York Academy of Sciences* **2012,** *1268* (1), 26-34.

18. Ghosh, A. K., Anaerobic Threshold: Its Concept and Role in Endurance Sport. *The Malaysian Journal of Medical Sciences : MJMS* **2004,** *11* (1), 24-36.

19. Clark, L. C.; Lyons, C., ELECTRODE SYSTEMS FOR CONTINUOUS MONITORING IN CARDIOVASCULAR SURGERY. *Annals of the New York Academy of Sciences* **1962,** *102* (1), 29-45.

20. (a) Chen, C.; Xie, Q.; Yang, D.; Xiao, H.; Fu, Y.; Tan, Y.; Yao, S., Recent advances in electrochemical glucose biosensors: a review. *RSC Advances* **2013,** *3* (14), 4473-4491; (b) Rassaei, L.; Olthuis, W.; Tsujimura, S.; Sudhölter, E. R.; van den Berg, A., Lactate biosensors: current status and outlook. *Anal Bioanal Chem* **2014,** *406* (1), 123-137.

21. (a) Malik, B. H.; Coté, G. L., Characterizing dual wavelength polarimetry through the eye for monitoring glucose. *Biomedical Optics Express* **2010,** *1* (5), 1247-1258; (b) Malik, B. H.; Pirnstill, C. W.; Coté, G. L., Dual-wavelength polarimetric glucose sensing in the presence of birefringence and motion artifact using anterior chamber of the eye phantoms. *BIOMEDO* **2013,** *18* (1), 017007-017007.

22. Esenaliev, R. O.; Larin, K. V.; Larina, I. V.; Motamedi, M., Noninvasive monitoring of glucose concentration with optical coherence tomography. *Opt. Lett.* **2001,** *26* (13), 992-994.

23. Caspers, P.; Lucassen, G.; Bruining, H.; Puppels, G., Detection of skin lactate by in vivo Raman spectroscopy. In *Spectroscopy of Biological Molecules: New Directions*, Greve, J.; Puppels, G. J.; Otto, C., Eds. Springer Netherlands: 1999; pp 485-486.

24. Kohl, M.; Essenpreis, M.; Böcker, D.; Cope, M., Influence of glucose concentration on light scattering intissue-simulating phantoms. *Opt. Lett.* **1994,** *19* (24), 2170-2172.

25. (a) O'Riordan, T. C.; Soini, A. E.; Papkovsky, D. B., Monofunctional Derivatives of Coproporphyrins for Phosphorescent Labeling of Proteins and Binding Assays. *Analytical Biochemistry* **2001,** *290* (2), 366-375; (b) Kürner, J. M.; Wolfbeis, O. S.; Klimant, I., Homogeneous Luminescence Decay Time-Based Assay Using Energy Transfer from Nanospheres. *Analytical Chemistry* **2002,** *74* (9), 2151-2156; (c) O'Sullivan, P. J.; Burke, M.; Soini, A. E.; Papkovsky, D. B., Synthesis and evaluation of phosphorescent oligonucleotide probes for hybridisation assays. *Nucleic Acids Research* **2002,** *30* (21), e114.

26. Smith, A. M.; Mancini, M. C.; Nie, S., Bioimaging: Second window for in vivo imaging. *Nat Nano* **2009,** *4* (11), 710-711.

27. (a) Roberts, J.; Collier, B. B.; McShane, M. J. In *Incorporation of optical enzymatic sensing chemistry into biocompatible hydrogels*, Sensors, 2011 IEEE, 28-31 Oct. 2011; 2011; pp 1245-1248; (b) McShane, M. J., Potential for Glucose Monitoring with Nanoengineered Fluorescent Biosensors. *Diabetes Technology & Therapeutics* **2002,** *4* (4), 533-538; (c) Chaudhary, A.; McShane, M. J.; Srivastava, R., Glucose response of dissolved-core alginate microspheres: towards a continuous glucose biosensor. *Analyst* **2010,** *135* (10), 2620-2628; (d) Brown, J. Q.; McShane, M. J., Modeling of spherical fluorescent glucose microsensor systems: Design of enzymatic smart tattoos. *Biosensors and Bioelectronics* **2006,** *21* (9), 1760-1769.

28. Roberts, J. R.; Park, J.; Helton, K.; Wisniewski, N.; McShane, M. J., Biofouling of Polymer Hydrogel Materials and its Effect on Diffusion and Enzyme-Based Luminescent Glucose Sensor Functional Characteristics. *Journal of Diabetes Science and Technology* **2012,** *6* (6), 1267-1275.

29. (a) Baker, D. A.; Gough, D. A., A Continuous, Implantable Lactate Sensor. *Analytical Chemistry* **1995,** *67* (9), 1536-1540; (b) Thomas, N.; Lähdesmäki, I.; Parviz, B. A., A contact lens with an integrated lactate sensor. *Sensors and Actuators B: Chemical* **2012,** *162* (1), 128-134; (c) Hu, A.-L.; Liu, Y.-H.; Deng, H.-H.; Hong, G.-L.; Liu, A.-L.; Lin, X.-H.; Xia, X.-H.; Chen, W., Fluorescent hydrogen peroxide sensor based on cupric oxide nanoparticles and its application for glucose and l-lactate detection. *Biosensors and Bioelectronics* **2014,** *61* (0), 374-378.

30. Choi, M. M. F., Progress in Enzyme-Based Biosensors Using Optical Transducers. *Microchim. Acta* **2004,** *148* (3-4), 107-132.

31. Marquette, C. A.; Leca, B. D.; Blum, L. J., Electrogenerated chemiluminescence of luminol for oxidase-based fibre-optic biosensors. *Luminescence* **2001,** *16* (2), 159-165.

32. Trettnak, W. W., Ottos, A Fiber Optic Lactate Biosensor with an Oxygen Optrode as the Transducer. *Analytical Letters* **1989,** *22* (9), 2191-2197.

33. Dremel, B. A. A.; Li, S. Y.; Schmid, R. D., On-line determination of glucose and lactate concentrations in animal cell culture based on fibre optic detection of oxygen in flow-injection analysis. *Biosensors and Bioelectronics* **1992,** *7* (2), 133-139.

34. Berezin, M. Y.; Achilefu, S., Fluorescence Lifetime Measurements and Biological Imaging. *Chemical Reviews* **2010,** *110* (5), 2641-2684.

35. (a) Niedermair, F.; Borisov, S. M.; Zenkl, G.; Hofmann, O. T.; Weber, H.; Saf, R.; Klimant, I., Tunable Phosphorescent NIR Oxygen Indicators Based on Mixed Benzo- and Naphthoporphyrin Complexes. *Inorganic Chemistry* **2010,** *49* (20), 9333-9342; (b) Koren, K.; Borisov, S. M.; Klimant, I., Stable optical oxygen sensing materials based on click-coupling of fluorinated platinum(II) and palladium(II) porphyrins—A convenient way to eliminate dye migration and leaching. *Sensors and Actuators B: Chemical* **2012,** *169* (0), 173-181.

36. To, W.-P.; Liu, Y.; Lau, T.-C.; Che, C.-M., A Robust Palladium(II)–Porphyrin Complex as Catalyst for Visible Light Induced Oxidative C□H Functionalization. *Chemistry – A European Journal* **2013,** *19* (18), 5654-5664.

37. Hoffman, A. S., Hydrogels for biomedical applications. *Advanced Drug Delivery Reviews* **2012,** *64, Supplement* (0), 18-23.

38. Lee, K. Y.; Mooney, D. J., Hydrogels for Tissue Engineering. *Chemical Reviews* **2001,** *101* (7), 1869-1880.

39. Uhrich, K. E.; Cannizzaro, S. M.; Langer, R. S.; Shakesheff, K. M., Polymeric Systems for Controlled Drug Release. *Chemical Reviews* **1999,** *99* (11), 3181-3198.

40. (a) Arciola, C. R.; Maltarello, M. C.; Cenni, E.; Pizzoferrato, A., Disposable contact lenses and bacterial adhesion. In vitro comparison between ionic/high-water-content and non-ionic/low-water-content lenses. *Biomaterials* **1995,** *16* (9), 685-690; (b) Ševčík, S.; Vacík, J.; Chmelíková, D.; Smetana, K., Jr., Surface alkaline hydrolysis of 2-hydroxyethyl methacrylate gels. *J Mater Sci: Mater Med* **1995,** *6* (9), 505-509.

41. Mohapatra, R.; Ray, D.; Swain, A. K.; Pal, T. K.; Sahoo, P. K., Release study of alfuzosin hydrochloride loaded to novel hydrogel P(HEMA-co-AA). *Journal of Applied Polymer Science* **2008,** *108* (1), 380-386.

42. (a) Jaiswal, M.; Koul, V., Assessment of multicomponent hydrogel scaffolds of poly(acrylic acid-2-hydroxy ethyl methacrylate)/gelatin for tissue engineering applications. *Journal of Biomaterials Applications* **2013,** *27* (7), 848-861; (b) Ramalingam, N.; Natarajan, T. S.; Rajiv, S., Development and Characterization of Electrospun Poly(2-hydroxy ethyl methacrylate) for Tissue Engineering Applications. *Advances in Polymer Technology* **2013,** *32* (3), n/a-n/a.

43. (a) Montheard, J.-P.; Chatzopoulos, M.; Chappard, D., 2-Hydroxyethyl Methacrylate (HEMA): Chemical Properties and Applications in Biomedical Fields. *Journal of Macromolecular Science, Part C* **1992,** *32* (1), 1-34; (b) Kochkodan, V. M.; Hilal, N.; Goncharuk, V. V.; Al-Khatib, L.; Levadna, T. I., Effect of the surface modification of polymer membranes on their microbiological fouling. *Colloid J* **2006,** *68* (3), 267-273; (c) Goli, K. K.; Rojas, O. J.; Genzer, J., Formation and Antifouling Properties of Amphiphilic Coatings on Polypropylene Fibers. *Biomacromolecules* **2012,** *13* (11), 3769-3779.

44. Peppas, N. A.; Moynihan, H. J.; Lucht, L. M., The structure of highly crosslinked poly(2-hydroxyethyl methacrylate) hydrogels. *Journal of Biomedical Materials Research* **1985,** *19* (4), 397-411.

45. (a) Raymond, S., ACRYLAMIDE GEL ELECTROPHORESIS. *Annals of the New York Academy of Sciences* **1964,** *121* (2), 350-365; (b) Akroyd, P., Acrylamide-gel Electrophoresis of [beta]-Lactoglobulins stored in Solutions at pH 8.7. *Nature* **1965,** *208* (5009), 488-489.

46. Ramaraj, B.; Radhakrishnan, G., Hydrogel capsules for sustained drug release. *Journal of Applied Polymer Science* **1994,** *51* (6), 979-988.

47. (a) Markvicheva, E. A.; Tkachuk, N. E.; Kuptsova, S. V.; Dugina, T. N.; Strukova, S. M.; Kirssh, Y. E.; Zubov, V. P.; Rumish, L. D., Stabilization of proteases by entrapment in a new composite hydrogel. *Appl Biochem Biotechnol* **1996,** *61* (1-2), 75-84; (b) Zhu, X.; Ma, Y.; Zhao, C.; Lin, Z.; Zhang, L.; Chen, R.; Yang, W., A Mild Strategy To Encapsulate Enzyme into Hydrogel Layer Grafted on Polymeric Substrate. *Langmuir* **2014,** *30* (50), 15229-15237.

48. (a) Stein, E. W.; Volodkin, D. V.; McShane, M. J.; Sukhorukov, G. B., Real-Time Assessment of Spatial and Temporal Coupled Catalysis within Polyelectrolyte Microcapsules Containing Coimmobilized Glucose Oxidase and Peroxidase. *Biomacromolecules* **2006,** *7* (3), 710-719; (b) Brown, J. Q.; Srivastava, R.; McShane, M. J., Encapsulation of glucose oxidase and an oxygen-quenched fluorophore in polyelectrolyte-coated calcium alginate microspheres as optical glucose sensor systems. *Biosensors and Bioelectronics* **2005,** *21* (1), 212-216.

49. Wan, L. S. C.; Heng, P. W. S.; Chan, L. W., Drug encapsulation in alginate microspheres by emulsification. *Journal of Microencapsulation* **1992,** *9* (3), 309-316.

50. Sukhorukov, G. B.; Donath, E.; Davis, S.; Lichtenfeld, H.; Caruso, F.; Popov, V. I.; Möhwald, H., Stepwise polyelectrolyte assembly on particle surfaces: a novel approach to colloid design. *Polymers for Advanced Technologies* **1998,** *9* (10-11), 759-767.

51. (a) Liam Andrus, R. U., Natalie Wisniewski, Michael McShane, Figure 1. Flow through system schematic. MDPI: Biosensors, 2015; (b) Andrus L., U. R., Wisniewski N., McShane M., Characterization of Lactate Sensors Based on Lactate Oxidase and Palladium Benzoporphyrin Immobilized in Hydrogels. *Biosensors* **2015,** *5* (3), 398-416.

52. Andrus L., U. R., Wisniewski N., McShane M., Figure 2. (a) Change of lactate concentration in permeate chamber over time for three sensor types; (b) Stern-Volmer plots for the same sensor types. Each set is an average of three compositionally identical sensors; errors bars denote 95% confidence intervals. MDPI: Biosensors, 2015.

53. Jitendra Solanski, S. G., Michael McShane, Sensitivity and Stability of Luminescent Oxygen Sensors based on poly(hydroxyethyl methacrylate) (pHEMA) Hydrogels with Encapsulated Palladium Benzoporphyrin. *In press* **2015**.

54. Andrus L., U. R., Wisniewski N., McShane M., Figure 3. (a) 75:25 pHEMA:pAam lifetime response to lactate interrogation (b) calibration curves for three sensor types. Each calibration curve contains points representing the average phosphorescent lifetime; error bars denote the 95% confidence intervals for n = 3 sensors. MDPI: Biosensors, 2015.

55. Baker, D. A.; Corkhill, P. H.; Ng, C. O.; Skelly, P. J.; Tighe, B. J., Synthetic hydrogels: 2. Copolymers of carboxyl-, lactam- and amide-containing monomers—structure/property relationships. *Polymer* **1988,** *29* (4), 691-700.

56. Andrus L., U. R., Wisniewski N., McShane M., Table 1. Compiled sensor metrics, values are average of three sensors ±95% confidence intervals. MDPU: Biosensors, 2015.

57. Andrus L., U. R., Wisniewski N., McShane M., Figure 4. (a) 90:10 pHEMA:pAam signal retention over 20 cycles (b) % retention of first cycle signal (c) % retention of fifth cycle signal. Markers indicate average values, and error bars represent 95% confidence intervals between measured signal retention for n = 3 sensors. MDPI: Biosensors, 2015.

58. Carreau, A.; Hafny-Rahbi, B. E.; Matejuk, A.; Grillon, C.; Kieda, C., Why is the partial oxygen pressure of human tissues a crucial parameter? Small molecules and hypoxia. *Journal of Cellular and Molecular Medicine* **2011,** *15* (6), 1239-1253.

59. (a) Ritter, D. W.; Roberts, J. R.; McShane, M. J., Glycosylation site-targeted PEGylation of glucose oxidase retains native enzymatic activity. *Enzyme and Microbial Technology* **2013,** *52* (4–5), 279-285; (b) Ritter, D. W.; Newton, J. M.; McShane, M. J., Modification of PEGylated enzyme with glutaraldehyde can enhance stability while avoiding intermolecular crosslinking. *RSC Advances* **2014,** *4* (53), 28036-28040.